

Wigner Function Shapelets I: formalism

Shun Arai *

Kobayashi-Maskawa Institute for the Origin of Particles and the Universe (KMI), Nagoya University, Nagoya, 464-8602, Japan

(Dated: February 3, 2026)

We extend shapelets for the analysis of galaxy images to be available in a phase space, introducing *Wigner Function Shapelets (WFS)*. Whereas conventional shapelets expand images separately in configuration or Fourier space using Hermite–Gaussian or Laguerre–Gaussian modes, WFS represents images directly in the four-dimensional phase space with symplectic group $\mathrm{Sp}(4, \mathbb{R})$, which is quantised by a phase-space cell $2\pi\lambda$ that determines a resolution limit of a telescope. WFS consists of a bilinear form of the cross-Wigner function of the Laguerre–Gaussian modes as an orthogonal and complete basis for the Wigner function of an image, carrying out $\mathrm{SU}(2)$ irreducible representations of the phase space with the Hopf tori. We introduce a scalar function $\mathcal{W}_{k\ell}(Q_0, Q_2)$ from the $\mathrm{U}(1) \times \mathrm{U}(1)$ - covariant tori to a two-dimensional space of constants of motion (Q_0, Q_2) —the harmonic energy and axial angular momentum—thereby yielding a natural phase–space “band structure”, given a pair of winding number $(k, \ell) \in \mathbb{Z}^2$. WFS leverage key properties of the Wigner function for image analysis: (i) it encodes full information of an image in a symmetry-preserving way; (ii) its transport equation naturally involves with a Liouville equation at $\lambda \rightarrow 0$; (iii) it admits positive/negative oscillatory patterns on (Q_0, Q_2) plane that can be sensitive spatial coherent structure of galaxy morphology and cosmological imprints; and (iv) systematics and noise can be manipulated as a quantum channel operation. This paper aims to bring all the formulae related to the Wigner function in the context of astrophysics and cosmology, formally organising in both terminologies of astronomy and of quantum information theory.

CONTENTS

I. Introduction	2	V. Practical usage in image analyses	18
II. Wigner function of galaxy images	3	A. Choice of σ	18
A. Basic properties	3	B. Choice of λ	19
B. Statistics for Wigner function	5	C. Existence of optimal recovery	20
1. Van Cittert–Zernike theorem, Wigner function, and speckle statistics	5	D. Feasibility	21
2. Statistical correlations over cosmological image ensemble	6	VI. Conclusions	21
C. Systematics and noise in Wigner function	7	Acknowledgments	22
1. Deterministic PSF	8	A. Classical limit of Wigner function and Wigner transport	22
2. Stochastic PSF	8	B. Wigner function for polarised/coloured images	23
III. Wigner Function Shapelets	9	C. Derivation of the PSF phase–space kernel by direct variable changes	23
A. Definition of Wigner Function Shapelets	9	D. Determination of the normalisation of WFS	24
B. Closed analytic form of WFS	10	E. Analytic relation between LG modes and spherical harmonics at small-angle limit	24
C. Hopf fibration of Wigner function	11	F. Weak-lensing operators with Swinger two oscillators	25
D. Morphology modes and rotation modes	13	a. Shear generator	25
1. Deterministic PSF	13	b. Flexion generator	25
2. Stochastic PSF	13	References	27
E. Correspondence between WFS and BiPoSHs representation	14		
F. Correspondence between WFS and FPFS	14		
IV. Cosmological information in Wigner function	16		
A. Shear response	16		
B. Flexion response	17		
C. Signals of parity violation	17		
D. Galaxy shape response to spin modes	18		

* shunarai@kmi.nagoya-u.ac.jp

I. INTRODUCTION

The shapelets formalism [1–4] has been widely employed to analyse the morphology of galaxies in two-dimensional configuration space, applied for extracting the shape distortion induced by weak gravitational lensing, i.e., cosmic shear (see the latest review in [5]) and flexions [6]. In 2018 [7] employed the shapelets to project the Fourier power function of a galaxy image in two-dimensional Fourier space, introducing the Fourier Power Function Shapelets (FPFS) method and accomplishing robust estimation of cosmic shear against measurement biases [8]. With the advent of high-resolution imaging surveys such as the James Webb Space Telescope (JWST), the Euclid mission, the Vera C. Rubin Observatory Legacy Survey of Space and Time (LSST), the Nancy Grace Roman Space Telescope (Roman), and the Square Kilometre Array Observatory (SKAO) [9–13], the analyses with shapelets continue to serve fiducial modelling so that any advanced methods can be validated and benchmarked [14–16].

The beauty of using shapelets, regardless of whether in configuration space or Fourier space, lies in their symmetry-preserving representation. In fact, a linear response to gravitational lensing is directly analogous to quantum transitions between angular-momentum eigenstates in the $SU(2)$ representation¹. In this framework, Hermite–Gaussian (HG) and Laguerre–Gaussian (LG) modes are simply two bases of the two-dimensional isotropic oscillator, labelled by total angular momentum $j = N/2$ (with N the total mode order) and spin quantum number s with $-j \leq s \leq j$ ²[17–19]. Gravitational lensing couples these states according to familiar selection rules: cosmic shear, generated by quadratic operators, induces transitions with $\Delta s = \pm 2$ at fixed j , while flexion, generated by cubic operators, produces $\Delta s = \pm 1$ and $\Delta s = \pm 3$. [2–4]. Because both HG and LG modes form infinite, orthogonal, and complete bases, related by $SU(2)$ rotations with amplitudes given by Wigner d –matrix elements [17–21], it is mathematically natural to employ shapelets to represent the information encoded in galaxy images with either HG or LG modes. This construction reflects the same completeness and orthogonality principles that underlie the Hilbert space of quantum mechanics [22, 23].

In this paper, we construct shapelets in the phase space described by the transverse coordinate on the image plane $\boldsymbol{\theta} = (\theta_x, \theta_y)$ and its conjugate momentum by $\boldsymbol{p} = (p_x, p_y)$, given the symplectic structure as $(\boldsymbol{\theta}, \boldsymbol{p}) \in \text{Sp}(4, \mathbb{R})$. In the phase space, a galaxy image is represented by its Wigner function [24]³, and then we will claim that the shapelets

¹ We describe the mode functions and the selection rules with $SU(2)$ representation in the whole paper. One can choose $SO(3)$ representation alternatively.

² Throughout this paper, we use s instead of m that has been commonly used in other papers in order to avoid the confusion when the spherical harmonics is labelled in Sec. II B 2.

³ The Wigner function is often referred to as the Wigner–Ville distribution, following the work of J. Ville in [25].

that expands the Wigner function of the image, *Wigner Function Shapelets* (WFS), provides a natural basis with preserving symplectic geometry [24, 26–29]. The Wigner function $W(\boldsymbol{\theta}, \boldsymbol{p})$ plays a central role in quantum physics as a quasi-probability distribution, namely the phase-space representation of the density operator which governs the evolution of a system in quantum mechanics. Hence it obeys the quantum Liouville (Moyal) flow that exhibits the conservation of information [30, 31], whose classical limit with $\hbar \rightarrow 0^4$ is nothing but the classical Liouville equation. Crucially, because the Wigner function is bilinear in the underlying field, the Wigner–Weyl transform provides a unitary correspondence, i.e., the Stratonovich–Weyl correspondence[33–36], between Hilbert–Schmidt operators on the underlying Hilbert space and square-integrable functions on phase space [26, 37, 38]. Within this representation, one can construct a Hilbert–Schmidt space spanned by the bilinear products of HG or LG modes. These modes, being orthogonal and complete by construction, offer a natural basis in which both image structure and its lensing-induced distortions can be decomposed and quantified, namely the WFS.

To extract the full information in the Wigner function, it is helpful to employ various mathematical tools in group representation in $SU(2)$. For instance, through the associated Hopf fibration of phase space [39], the Hilbert–Schmidt space decomposes naturally into diagonal sectors, depending only on the invariants (Q_0, Q_2) —the harmonic energy and axial angular momentum—and off-diagonal sectors, which arrange into torus harmonics. The diagonal sector encodes number–state content, while the off-diagonal coherences form band structures that isolate spin components relevant for image deformations, all while retaining locality in $(\boldsymbol{\theta}, \boldsymbol{p})$. The non-local or topological information are embedded into Hopf-torus phases distinguished by a pair of torus-winding numbers $(k, \ell) \in \mathbb{Z}^2$. Thus, the Wigner representation of the image not only embeds galaxy images in phase space but also exposes the underlying group–theoretic architecture of their shape decomposition, including non-local and topological information. In other words, the Wigner function encapsulates correlations between configuration and Fourier space that are inaccessible to analyses carried out in either domain alone.

It is important to note that the decomposition of the Wigner function in phase space is not a new idea: it has long been developed in quantum optics to characterise laser-beam morphology [17, 21, 26, 40, 41], within the paraxial approximation to the Helmholtz equation derived from Maxwell’s equations. The novelty of our work lies in transposing that formalism into the morphological analysis of galaxy images, which can likewise be modelled by paraxial propagation equations in observations of

⁴ In this paper, we introduce λ instead of \hbar that denotes the scale where “quantisation” of the image is given, following the notation [32]. We will describe this in more detail in Sec. V B.

distant galaxies by telescopes[42–44], and in introducing the concept of WFS into the astrophysical context. We anticipate that this framework may open fertile avenues of interplay between quantum optics and astrophysics ahead the future astronomical observations.

The rest of the paper is organised as follows. In Sec. II we will describe what the Wigner function of a galaxy image is, given the basic properties of the Wigner function. We will mention statistics and modulation of the Wigner function under systematics and noises, clarifying the relation between the Wigner function supported by the quantum information theory and the conventional astrophysical concepts in image analysis. In Sec. III, we will introduce the formalism of WFS and introduce the topologically-sensitive observable $\mathcal{W}_{k\ell}$. In Sec. IV, we will make use of the Wigner function and the WFS to characterise the linear response to weak gravitational lensing and galaxy shape responses to any higher spin modes. We will give an observable that is sensitive to parity-violating signatures in galaxy-shape angular correlations. In Sec. V, we will argue how the WFS is applied for practical image analysis, prescribing modest choices of the galaxy size parameter σ and the one-dimensional phase-space cell $2\pi\lambda$. Finally, we will conclude our paper. Technical materials are collected in the appendices, supplying sufficient information that are necessary to understand the formulae in the main text.

II. WIGNER FUNCTION OF GALAXY IMAGES

Our theme is to analyse a galaxy image in phase space with the Wigner function, thereby extracting morphological information beyond what is accessible in configuration or Fourier space separately. In this section we define the Wigner function for an image field of a measured galaxy and summarise its essential mathematical properties given the Wigner function. We clarify how the Wigner function is related to the conventional astrophysical statistics, systematics, and noises.

A. Basic properties

Let us consider the image plane with the coordinate $\boldsymbol{\theta} = (\theta_x, \theta_y)$. The phase space associated with the image plane is defined by introducing the conjugate momentum $\mathbf{p} = (p_x, p_y)$ and the symplectic structure as $\text{Sp}(4, \mathbb{R})$: $\{S \in GL(4, \mathbb{R}) \mid S^T \Omega S = \Omega\}$ where

$$\Omega = \begin{pmatrix} 0 & I_2 \\ -I_2 & 0 \end{pmatrix}, \quad (1)$$

with I_2 is the 2×2 identity. $\text{Sp}(4, \mathbb{R})$ contains translations, rotations, squeezes, and more general linear canonical transforms, all of which relates physical deformation of an image.

Let us consider an image field of a galaxy $\psi(\boldsymbol{\theta})$. In practice, $\psi(\boldsymbol{\theta})$ is often a real positive function as it loses

phase information of electrocmagnetic fields, but we treat $\psi(\boldsymbol{\theta})$ as an arbitrary field that can be complex in general. The Wigner function of the image is defined as

$$W(\boldsymbol{\theta}, \mathbf{p}) \equiv \frac{1}{(2\pi\lambda)^2} \int d^2\boldsymbol{\xi} \psi(\boldsymbol{\theta} + \boldsymbol{\xi}/2) \psi^*(\boldsymbol{\theta} - \boldsymbol{\xi}/2) e^{-\frac{i\mathbf{p}\cdot\boldsymbol{\xi}}{\lambda}}. \quad (2)$$

Here λ is the scale of the discretisation of phase space that determines the canonical commutation relations

$$[\hat{\theta}_i, \hat{p}_j] = i\lambda\delta_{ij}, [\hat{\theta}_i, \hat{\theta}_j] = [\hat{p}_i, \hat{p}_j] = 0, \quad (3)$$

with $i, j = x, y$. The Wigner function defined by Eq. (2) obeys several well-known properties as follows.

Reality $W(\boldsymbol{\theta}, \mathbf{p}) \in \mathbb{R}$ for any $\psi(\boldsymbol{\theta})$

Parity The Wigner function is invariant under the parity transform in phase space as

$$\hat{\Pi}W(\boldsymbol{\theta}, \mathbf{p}) = W(\boldsymbol{\theta}, \mathbf{p}), \quad (4)$$

where $\hat{\Pi}$ acts as reflection in phase space, $\hat{\Pi}A(\boldsymbol{\theta}, \mathbf{p}) = A(-\boldsymbol{\theta}, -\mathbf{p})$.

Chirality The Wigner function is invariant under the chiral transform in the phase space;

$$\hat{C}W(\boldsymbol{\theta}, \mathbf{p}) = W(\boldsymbol{\theta}, \mathbf{p}), \quad (5)$$

where \hat{C} acts as reflection in phase space, $\hat{C}A(\boldsymbol{\theta}, \mathbf{p}) = A(\boldsymbol{\theta}, -\mathbf{p})$. Since the Wigner function of the single image is always real, the image itself preserves the chirality.

Symplectic covariance Let $S \in \text{Sp}(4, \mathbb{R})$ act on phase-space points $z = (\boldsymbol{\theta}, \mathbf{p})$ as $z \mapsto Sz$. We adopt the pullback convention $\hat{S}F(z) \equiv F(S^{-1}z)$. Then the Wigner map is covariant under any linear canonical (symplectic) transformation:

$$W \mapsto \hat{S}W, \quad S \in \text{Sp}(4, \mathbb{R}).$$

Note that translations, rotations, shears, squeezes are all included.

Weyl symbols and expectations Let us define the state $\hat{\rho}$ for the galaxy field with the kernel $\rho(\boldsymbol{\theta}_1, \boldsymbol{\theta}_2) = \psi(\boldsymbol{\theta}_1)\psi^*(\boldsymbol{\theta}_2)$. An observable \hat{A} with kernel $A(\boldsymbol{\theta}_1, \boldsymbol{\theta}_2)$ define the Weyl symbol of \hat{A} as

$$A_W(\boldsymbol{\theta}, \mathbf{p}) = \int d^2\boldsymbol{\xi} A\left(\boldsymbol{\theta} + \frac{\boldsymbol{\xi}}{2}, \boldsymbol{\theta} - \frac{\boldsymbol{\xi}}{2}\right) e^{-\frac{i\mathbf{p}\cdot\boldsymbol{\xi}}{\lambda}}. \quad (6)$$

Then the expectation value is the phase-space inner product

$$\langle \hat{A} \rangle = \text{Tr}(\hat{\rho} \hat{A}) = \int d\mu(\boldsymbol{\theta}, \mathbf{p}) A_W(\boldsymbol{\theta}, \mathbf{p}) W(\boldsymbol{\theta}, \mathbf{p}). \quad (7)$$

Here $d\mu(\boldsymbol{\theta}, \mathbf{p}) \equiv d^2\boldsymbol{\theta} d^2\mathbf{p}$ denotes the Liouville measure. If $\text{Tr} \hat{\rho} = 1$ then $\int d\mu W = 1$. Although W may take negative values, W is called as a "quasi" probability density.

Wigner transport Suppose that the galaxy field can evolve along an optical path s , namely $\psi(\boldsymbol{\theta}, s)$. Let \hat{H} be the generator of evolution along an optical path parameter s , and $H_W(\boldsymbol{\theta}, \mathbf{p}, s)$ its Weyl symbol. The Moyal (star) product on the phase space is defined between the two Weyl symbols as

$$A_W \star B_W = A_W \exp\left[\frac{i\lambda}{2} \overleftrightarrow{\Lambda}\right] B_W, \quad \overleftrightarrow{\Lambda} \equiv \overleftarrow{\nabla}_{\boldsymbol{\theta}} \cdot \overrightarrow{\nabla}_{\mathbf{p}} - \overleftarrow{\nabla}_{\mathbf{p}} \cdot \overrightarrow{\nabla}_{\boldsymbol{\theta}}, \quad (8)$$

and the associated Moyal bracket is

$$\{A_W, B_W\}_{\text{MB}} = \frac{2}{\lambda} A_W \sin\left(\frac{\lambda}{2} \overleftrightarrow{\Lambda}\right) B_W. \quad (9)$$

The von–Neumann equation $i\lambda \partial_s \hat{\rho} = [\hat{\rho}, \hat{H}]$ maps to the exact Wigner transport as

$$\partial_s W(\boldsymbol{\theta}, \mathbf{p}, s) = \{W, H_W\}_{\text{MB}}. \quad (10)$$

Expanding the sine in the limit of $\lambda \rightarrow 0$ gives the classical Liouville equation as

$$\begin{aligned} \partial_s W &= \{W, H_W\}_{\text{PB.}} + \mathcal{O}(\lambda^2), \\ \{W, H\}_{\text{PB.}} &= \nabla_{\boldsymbol{\theta}} W \cdot \nabla_{\mathbf{p}} H_W - \nabla_{\mathbf{p}} W \cdot \nabla_{\boldsymbol{\theta}} H_W. \end{aligned} \quad (11)$$

Note that this is a generalisation of the radiative-transfer equation of an image, including the phase-space information. In App. A, we derive that H_W matches the classical Hamiltonian and the Wigner function approaches the spectral radiance $L(\boldsymbol{\theta}, \mathbf{p})$.

Duality to characteristic function The Wigner function $W(\boldsymbol{\theta}, \mathbf{p})$ is the phase-space representation dual to the Weyl characteristic function, which serves as the fundamental generating an object of the image density matrix. Defining the characteristic function as the expectation value of the phase-space displacement operator,

$$\chi(\boldsymbol{\eta}, \boldsymbol{\zeta}) := \text{Tr} \left[\hat{\rho} \exp\left(\frac{i}{\lambda} (\boldsymbol{\eta} \cdot \hat{\boldsymbol{\theta}} + \boldsymbol{\zeta} \cdot \hat{\mathbf{p}})\right) \right]. \quad (12)$$

One finds that χ generates all symmetrised moments of the canonical variables and encodes both the probabilistic content (diagonal part) and the coherence structure (off-diagonal part) of the density matrix. The Wigner function is obtained by a Fourier transform of χ with respect to the source variables,

$$W(\boldsymbol{\theta}, \mathbf{p}) = \frac{1}{(2\pi\lambda)^2} \int d^2\boldsymbol{\eta} d^2\boldsymbol{\zeta} \chi(\boldsymbol{\eta}, \boldsymbol{\zeta}) e^{-\frac{i}{\lambda}(\boldsymbol{\eta}\boldsymbol{\theta} + \boldsymbol{\zeta}\mathbf{p})}, \quad (13)$$

while the inverse relation reconstructs χ from W by the inverse Fourier transformation. This establishes a one-to-one duality between the density matrix $\hat{\rho}$, its characteristic function χ , and the Wigner function W , showing that the latter is not an independent object but a coordinate representation of the same underlying statistical state.

Marginals The marginalisation of the Wigner function Eq. (2) derive the well-known quantities. The integration over the configuration space gives the Fourier power spectrum of $\psi(\boldsymbol{\theta}) : F(\mathbf{k}) = |\tilde{\psi}(\mathbf{k})|^2$ at $\mathbf{k} = \mathbf{p}/\lambda$ as,

$$F(\mathbf{p}/\lambda) = \int d^2\boldsymbol{\theta} W(\boldsymbol{\theta}, \mathbf{p}), \quad (14)$$

whereas the integration over the momentum space gives the intensity of $\psi(\boldsymbol{\theta}) : I(\boldsymbol{\theta}) = |\psi(\boldsymbol{\theta})|^2$ as

$$I(\boldsymbol{\theta}) = \int d^2\mathbf{p} W(\boldsymbol{\theta}, \mathbf{p}). \quad (15)$$

Note that the normalisation for the intensity is fixed at the limit $\lambda \rightarrow 0$, so that corresponding to the standard normalisation. One can see that the information in the phase space described by the Wigner function is marginalised into either $F(\mathbf{p}/\lambda)$ and $I(\boldsymbol{\theta})$. In other words, the direct analysis of the Wigner function in the phase space can possess the information that is integrated out in these marginals.

The Wigner function in Eq. (2) is computed with the single function. In other words, we assume that a galaxy image at one certain filter in colours or fixed polarisation, therefore the image is a single function. In general, one can obtain multiple images of the same source galaxy with different colour bands and polarisations. Moreover, even for a single image, the expansion of the Wigner function with a certain basis e.g. HG modes or LG modes, creates cross-terms in different quantum numbers and indeed these are non-zero at local points in the phase space. To make the image analysis complete in the phase space, such cross terms must be taken into account, we must be careful that some leakage occurs in image reconstruction. After all, it is significant to introduce the cross-Wigner function as follows. The cross-Wigner function is defined with the two different functions $\psi_a(\boldsymbol{\theta})$ and $\psi_b(\boldsymbol{\theta})$ as

$$W_{ab}(\boldsymbol{\theta}, \mathbf{p}) \equiv \frac{1}{(2\pi\lambda)^2} \int d^2\xi \psi_a(\boldsymbol{\theta} + \boldsymbol{\xi}/2) \psi_b^*(\boldsymbol{\theta} - \boldsymbol{\xi}/2) e^{-\frac{i\mathbf{p}\cdot\boldsymbol{\xi}}{\lambda}}. \quad (16)$$

Note that the abstract indices a, b can be the pair of the quantum number as $a = (j, s)$, as well as denoting multiple states of a source galaxy. It is sesquilinear (linear in ψ_a and conjugate-linear in ψ_b), satisfies $W_{ba} = W_{ab}^*$ and reduces to the ordinary Wigner function when $a = b$. Note that the cross-Wigner function is no longer parity invariant by definition unless $a = b$.

The covariance of the Wigner function is not that simple compared to Eq. (2), but it is still defined in a covariant manner. For any unitary U acting on fields (so the indices transform as $(a, b) \mapsto (Ua, Ub)$), the cross-Wigner function covariantly transform as

$$W_{Ua, Ub}(z) = \begin{cases} W_{ab}(z - \boldsymbol{\zeta}), & U = D(\boldsymbol{\zeta}) \\ W_{ab}(S^{-1}z), & U = \mu(S), \end{cases} \quad (17)$$

where $D(\zeta)$ and $\mu(S)$ denotes the Heisenberg-Weyl displacement and the metaplectic transformations, respectively. Note that the linear transformation between HG \leftrightarrow LG modes via the Wigner d -matrix is one of the metaplectic transform. There is another deformation of polarisation is described by a unitary transform U in $SU(2)$. For instance, the Faraday rotation is described by this group of unitary operations, realising the covariance of the cross-Wigner function. The transform between images in colours of the single galaxy, in contrast, is not in general unitary because it may include diffusion, absorption, emission, convolution with instruments and atmospheric effects. Nevertheless these effects may be built in the cross-Wigner transport equation along the optical path s as a straightforward extension of the Wigner transport Eq. (10) with open system e.g. the Lindbladian (see a short review in [45]). In this paper, we focus in employing the cross-Wigner function to complete the basis representation in the phase space.

The marginals reproduce cross kernels:

$$\begin{aligned} \int d^2\mathbf{p} W_{ab}(\boldsymbol{\theta}, \mathbf{p}) &= \psi_a(\boldsymbol{\theta}) \psi_b^*(\boldsymbol{\theta}), \\ \int d^2\boldsymbol{\theta} W_{ab}(\boldsymbol{\theta}, \mathbf{p}) &= \tilde{\psi}_a(\mathbf{p}/\lambda) \tilde{\psi}_b^*(\mathbf{p}/\lambda), \end{aligned} \quad (18)$$

and, with the normalisation in (16), the total integral yields the inner product

$$\int d\mu(\boldsymbol{\theta}, \mathbf{p}) W_{ab}(\boldsymbol{\theta}, \mathbf{p}) = \langle \psi_b | \psi_a \rangle, \quad (19)$$

where the inner product is defined as

$$\langle \psi_b | \psi_a \rangle \equiv \int d^2\boldsymbol{\theta} \psi_a(\boldsymbol{\theta}) \psi_b^*(\boldsymbol{\theta}). \quad (20)$$

There is Moyal/Plancherel identity as

$$\langle W_{cd} | W_{ab} \rangle_{\text{HS}} = \frac{1}{(2\pi\lambda)^2} \langle \psi_a | \psi_c \rangle \langle \psi_b | \psi_d \rangle, \quad (21)$$

where we introduce the inner product in a Hilbert-Schmidt space as

$$\langle B | A \rangle_{\text{HS}} \equiv \text{Tr}(\hat{B}^\dagger \hat{A}) = \int d\mu A_W(z) B_W^*(z). \quad (22)$$

The identity Eq. (21) is used to project a Wigner function onto the basis function in the next section.

Let us comment on the uniqueness of the Wigner function. Given the Stratonovich-Wigner axioms: translation covariance, Hermiticity/self-duality, standardisation, metaplectic covariance, the kernel is uniquely fixed (up to the sign set by exact marginals) to be the displaced parity. Hence, the Stratonovich-Weyl correspondence [34] built from parity-reflected displacements is identical to the Wigner transform used in Eq. (2):

$$\hat{w}(z) = \hat{D}(z) \hat{\Pi} \hat{D}(z)^\dagger, \quad (23)$$

and this defines the Wigner function as $W = \text{Tr}[\hat{\rho} \hat{w}]$ given the state $\hat{\rho}$.

B. Statistics for Wigner function

We describe several statistical quantities derived from the Wigner function, recalling that the Wigner function is a phase-space quasi-probability distribution of an underlying state described by a density matrix of a galaxy image. We aim to organise this section so that the concept of the Wigner function fits into the conventional astrophysical quantities.

1. Van Cittert-Zernike theorem, Wigner function, and speckle statistics

We summarise how the Van Cittert-Zernike (VCZ) theorem [46, 47], statistical optics [48], and speckle statistics [49, 50] are unified in the Wigner-function representation adopted in this work, following a concise derivation in [51]. In the context of astronomical imaging, the VCZ theorem states how electromagnetic waves emitted from an astronomical body turn into an observable at a detector or a telescope. Statistics optics treats the persistence of the same astronomical body on the image plane by averaging a chunk of images that can fluctuate on the image plane over observational time. Speckle statistics is one of the popular representations of statistical optics, which formalises the statistical displacement of each image of the same astronomical body in a resolved time period. In what follows, we describe how naturally these quantities are harnessed by the Wigner function.

Let us assume that astronomical sources emit spatially incoherent (thermal) electromagnetic-wave radiation⁵. The image field $\psi(\boldsymbol{\theta})$ is treated as a product through random complex processes, and its second-order statistics are encoded in the mutual intensity (cross-spectral density)

$$\Gamma(\boldsymbol{\theta}_1, \boldsymbol{\theta}_2) \equiv \langle \psi(\boldsymbol{\theta}_1) \psi^*(\boldsymbol{\theta}_2) \rangle_{\text{obs.}}, \quad (24)$$

where $\langle \dots \rangle_{\text{obs.}}$ denotes an ensemble (or ergodic time) average over statistically equivalent field realisations. Inserting the image field ψ into the definition of the Wigner function generates the Wigner function. Ensemble averaging over the time-varying electromagnetic field yields the Weyl transform of the mutual intensity,

$$\langle W(\boldsymbol{\theta}, \mathbf{p}) \rangle_{\text{obs.}} = \frac{1}{(2\pi\lambda)^2} \int d^2\boldsymbol{\xi} \Gamma\left(\boldsymbol{\theta} + \frac{\boldsymbol{\xi}}{2}, \boldsymbol{\theta} - \frac{\boldsymbol{\xi}}{2}\right) e^{-i\frac{\mathbf{p}\cdot\boldsymbol{\xi}}{\lambda}}. \quad (25)$$

⁵ One may wonder whether the spatial structure of an observed astronomical object is spatially coherent; spirals, bars, jets etc. What we note here is the incoherence of the radiation, and the spatial structures remain spatially coherent with dependence of resolution of images.

Eq. (25) is inverted by the Fourier transform, and we obtain

$$\Gamma\left(\boldsymbol{\theta} + \frac{\boldsymbol{\xi}}{2}, \boldsymbol{\theta} - \frac{\boldsymbol{\xi}}{2}\right) = \int d^2\mathbf{p} \langle W(\boldsymbol{\theta}, \mathbf{p}) \rangle_{\text{obs.}}. \quad (26)$$

Eq. (26) indicates that the mutual information is a marginal of the ensemble-averaged Wigner function. Let us further assume that the observed image is no longer spatially incoherent due to strong image blurring in observational time, namely, the detailed structures are smoothed away. In this extreme case, the mutual intensity is reduced to the brightness distribution $I_S(\boldsymbol{\beta})$, the VCZ theorem implies that the mutual intensity at the telescope is the Fourier transform of the source intensity,

$$\Gamma\left(\boldsymbol{\theta} + \frac{\boldsymbol{\xi}}{2}, \boldsymbol{\theta} - \frac{\boldsymbol{\xi}}{2}\right) = \int d^2\boldsymbol{\beta} I_S(\boldsymbol{\beta}) e^{-\frac{i}{\lambda}\boldsymbol{\beta}\cdot\boldsymbol{\xi}}, \quad (27)$$

where $\boldsymbol{\xi}$ is the angular separation variable. The propagation distance does not appear explicitly, as the geometry is fully encoded in angular coordinates. Substituting Eq. (27) gives

$$\langle W(\boldsymbol{\theta}, \mathbf{p}) \rangle_{\text{obs.}} \propto I_S(\mathbf{p}), \quad (28)$$

showing that, for an incoherent source, the ensemble-averaged Wigner function is independent of $\boldsymbol{\theta}$ and directly encodes the source brightness in the conjugate-momentum space.

A single observed image corresponds to one realisation of the random field $\psi(\boldsymbol{\theta})$ and exhibits speckle due to random phase interference. Let us define the intensity of the image field is

$$I(\boldsymbol{\theta}) \equiv |\psi(\boldsymbol{\theta})|^2. \quad (29)$$

Its ensemble mean is given by the diagonal of the mutual intensity,

$$\langle I(\boldsymbol{\theta}) \rangle_{\text{obs.}} = \Gamma(\boldsymbol{\theta}, \boldsymbol{\theta}) = \int d^2\mathbf{p} \langle W(\boldsymbol{\theta}, \mathbf{p}) \rangle_{\text{obs.}}. \quad (30)$$

Speckle fluctuations are quantified by the intensity-intensity correlation function

$$G^{(2)}(\boldsymbol{\theta}_1, \boldsymbol{\theta}_2) \equiv \langle I(\boldsymbol{\theta}_1) I(\boldsymbol{\theta}_2) \rangle_{\text{obs.}}. \quad (31)$$

If the field ψ is a circular complex Gaussian random process (fully -developed speckle), the fourth-order moments reduce via the Siegert relation [52–55]⁶,

$$\langle I(\boldsymbol{\theta}_1) I(\boldsymbol{\theta}_2) \rangle_{\text{obs.}} = \langle I(\boldsymbol{\theta}_1) \rangle_{\text{obs.}} \langle I(\boldsymbol{\theta}_2) \rangle_{\text{obs.}} + |\Gamma(\boldsymbol{\theta}_1, \boldsymbol{\theta}_2)|^2. \quad (32)$$

The Siegert relation can be written entirely in terms of the ensemble-averaged Wigner function,

$$\begin{aligned} \langle I(\boldsymbol{\theta}_1) I(\boldsymbol{\theta}_2) \rangle &= \langle I(\boldsymbol{\theta}_1) \rangle \langle I(\boldsymbol{\theta}_2) \rangle \\ &+ \left| \int d^2\mathbf{p} \langle W\left(\frac{\boldsymbol{\theta}_1+\boldsymbol{\theta}_2}{2}, \mathbf{p}\right) \rangle_{\text{obs.}} e^{+i\frac{\mathbf{p}\cdot(\boldsymbol{\theta}_1-\boldsymbol{\theta}_2)}{\lambda}} \right|^2. \end{aligned} \quad (33)$$

Eqs. (28)–(33) make explicit that the VCZ theorem fixes the ensemble-averaged background Wigner distribution, while speckle arises from higher-order statistics of single realisations and is governed by the modulus-squared coherence encoded in $\langle W \rangle_{\text{obs.}}$. Throughout the rest of the main text, we implicitly consider the statistical ensemble over an observational time window, and we abbreviate the notation of the ensemble until it is necessary to show.

2. Statistical correlations over cosmological image ensemble

We consider a cosmological ensemble of galaxy images whose centroids are located at directions $\mathbf{n}_c \in S^2$. Around each centroid, we introduce local tangent-plane coordinates and define two nearby directions

$$\mathbf{n}_\pm \equiv \exp_{\mathbf{n}_c} \left(\boldsymbol{\theta} \pm \frac{\boldsymbol{\xi}}{2} \right), \quad |\boldsymbol{\theta}|, |\boldsymbol{\xi}| \ll 1, \quad (34)$$

where $\boldsymbol{\theta}$ and $\boldsymbol{\xi}$ denote small angular separations orthogonal to \mathbf{n}_c . The local Wigner function associated with the image field $\psi(\mathbf{n}) = \psi(\boldsymbol{\theta}; \mathbf{n}_c)$ is rewritten as

$$W(\boldsymbol{\theta}, \mathbf{p}; \mathbf{n}_c) = \frac{1}{(2\pi\lambda)^2} \int d^2\boldsymbol{\xi} \psi(\mathbf{n}_+) \psi^*(\mathbf{n}_-) e^{-\frac{i\mathbf{p}\cdot\boldsymbol{\xi}}{\lambda}}, \quad (35)$$

which is the Fourier transform, with respect to the relative angular separation $\boldsymbol{\xi} = \mathbf{n}_+ - \mathbf{n}_-$ of the local configuration-space bilinear. Taking an ensemble average over realisations of the cosmological image field yields

$$\langle W(\boldsymbol{\theta}, \mathbf{p}; \mathbf{n}_c) \rangle_{\text{cosmo.}} = \frac{1}{(2\pi\lambda)^2} \int d^2\boldsymbol{\xi} C(\mathbf{n}_+, \mathbf{n}_-) e^{-\frac{i\mathbf{p}\cdot\boldsymbol{\xi}}{\lambda}}, \quad (36)$$

where

$$C(\mathbf{n}, \mathbf{n}') \equiv \langle \psi(\mathbf{n}) \psi^*(\mathbf{n}') \rangle_{\text{cosmo.}}, \quad (37)$$

is the two-point angular correlation function of the ensemble. The correlation function on the sphere admits a complete expansion as

$$C(\mathbf{n}, \mathbf{n}') = \sum_{\ell_1 \ell_2} \sum_{LM} A_{\ell_1 \ell_2}^{LM} \left\{ Y_{\ell_1} \otimes Y_{\ell_2} \right\}_{LM}(\mathbf{n}, \mathbf{n}'), \quad (38)$$

where $\ell_{1,2}$ are the multipole moments and $m_{1,2}$ are magnetic quantum numbers, involving a total azimuthal quantum number L and a total magnetic quantum number M as $|\ell_1 - \ell_2| \leq L \leq \ell_1 + \ell_2$ and $M = m_1 + m_2$. $\{Y_{\ell_1} \otimes Y_{\ell_2}\}_{LM}$

⁶ In optics, the Siegert relation is often written with a normalised version in which the first term in the right-hand side of Eq. (32) is unity.

denotes the bipolar spherical harmonics (BiPoSHs) [56–58] that is defined as

$$\begin{aligned} & \{Y_{\ell_1} \otimes Y_{\ell_2}\}_{LM}(\mathbf{n}, \mathbf{n}') \\ &= \sum_{m_1, m_2} \langle \ell_1 m_1 \ell_2 m_2 | LM \rangle Y_{\ell_1 m_1}(\mathbf{n}) Y_{\ell_2 m_2}(\mathbf{n}'). \end{aligned} \quad (39)$$

Note that $\langle \ell_1 m_1 \ell_2 m_2 | LM \rangle$ is Clebsch-Gordan coefficients. The inversion of the bipolar spherical harmonics is derived as

$$Y_{\ell_1, m_1}(\mathbf{n}) Y_{\ell_2, m_2}(\mathbf{n}') = \sum_{LM} \langle \ell_1 m_1 \ell_2 m_2 | LM \rangle \{Y_{\ell_1} \otimes Y_{\ell_2}\}_{LM}. \quad (40)$$

After projecting out the basis, $A_{\ell_1 \ell_2}^{LM}$ is represented as

$$A_{\ell_1 \ell_2}^{LM} = \sum_{m_1, m_2} \langle a_{\ell_1 m_1} a_{\ell_2 m_2}^* \rangle_{\text{cosmo.}} \langle \ell_1 m_1 \ell_2 - m_2 | LM \rangle \quad (41)$$

where $a_{\ell m}$ denotes the multipole coefficient for the expansion of ψ . $A_{\ell_1 \ell_2}^{LM}$ encode the statistical anisotropy of the ensemble. In the statistically isotropic limit, only the $L = 0$ component survives, reproducing the usual angular power spectrum. Substituting Eq. (38) into Eq. (36), we obtain

$$\langle W(\boldsymbol{\theta}, \mathbf{p}; \mathbf{n}_c) \rangle_{\text{cosmo.}} = \sum_{\ell_1 \ell_2} \sum_{LM} A_{\ell_1 \ell_2}^{LM} \mathcal{K}_{\ell_1 \ell_2}^{LM}(\boldsymbol{\theta}, \mathbf{p}; \mathbf{n}_c), \quad (42)$$

where the kernel

$$\mathcal{K}_{\ell_1 \ell_2}^{LM} \equiv \frac{1}{(2\pi\lambda)^2} \int d^2\boldsymbol{\xi} \left\{ Y_{\ell_1} \otimes Y_{\ell_2} \right\}_{LM}(\mathbf{n}_+, \mathbf{n}_-) e^{-\frac{i\mathbf{p}\cdot\boldsymbol{\xi}}{\lambda}}, \quad (43)$$

acts as a phase-space response function relating bipolar angular correlations to the local Wigner representation. Eq. (42) demonstrates that the ensemble-averaged Wigner function naturally inherits decomposition with BiPoSHs. This provides a direct bridge between cosmological two-point statistics on the sphere and local phase-space descriptions of galaxy images. One can apply the same logic for the cross-Wigner function.

At last, let us briefly mention the two-point angular correlation of the Wigner function composed of the two galaxy images, $\langle W_{11}(\mathbf{n}_{c1}) W_{22}(\mathbf{n}_{c2}) \rangle_{\text{cosmo.}}$, setting the same lab frame of the two images. Note that are the galaxies are located at \mathbf{n}_{c1} and \mathbf{n}_{c2} , respectively. We obtain that $\langle W_{11}(\mathbf{n}_{c1}) W_{22}(\mathbf{n}_{c2}) \rangle_{\text{cosmo.}}$ is composed of the four-point correlation functions of the galaxy images, including the trispectrum of the galaxy image. We shall not show any detailed expression of the formula to keep the presentation concise, whereas we adhere to the essential meaning of such an ensemble. In practice, one may be interested in the configuration in which the two galaxy samples are distant compared to their own size,

namely $|\mathbf{n}_{c1} - \mathbf{n}_{c2}| \gg |\boldsymbol{\theta}|$. In this case, the four-point correlation function takes its collapsed limit cf. [59] in Fourier space. In Sec. IV, we will utilise $\langle W_{ab} \rangle_{\text{cosmo.}}$ to measure the cosmic shear as the standard analysis for weak gravitational lensing does. In addition, we will mention that one can build a parity-violating estimator within $\langle W_{11}(\mathbf{n}_{c1}) W_{22}(\mathbf{n}_{c2}) \rangle_{\text{cosmo.}}$, after projecting into the spin-sensitive observables that are defined in Sec. IV D.

C. Systematics and noise in Wigner function

We introduce systematics and noises on a galaxy image in terms of the Wigner function. Respecting that the Wigner function is the phase-space representation of an image state $\hat{\rho}$, we describe systematics and noises with corresponding algebraic operations in quantum information theory. To begin with this subsection, we provide a generic operation that characterises systematics and noises. Then we exemplify the two typical cases divided by whether the PSF is deterministic or stochastic.

A physical process acting on a state $\hat{\rho}$ is represented by a completely positive trace-preserving (CPTP) map,

$$\mathcal{E} : \hat{\rho} \longmapsto \mathcal{E}(\hat{\rho}). \quad (44)$$

Any CPTP map admits a Kraus representation,

$$\mathcal{E}(\hat{\rho}) = \sum_a \hat{K}_a \hat{\rho} \hat{K}_a^\dagger, \quad \sum_a \hat{K}_a^\dagger \hat{K}_a = \hat{\mathbb{I}}, \quad (45)$$

where $\{\hat{K}_a\}$ are Kraus operators. The representation may involve a discrete or continuous index. In particular, the continuous case is define as

$$\mathcal{E}(\hat{\rho}) = \int d\mu \hat{K}(z) \hat{\rho}(z) \hat{K}^\dagger(z), \quad \int d\mu \hat{K}(z) \hat{K}^\dagger(z) = \hat{\mathbb{I}}. \quad (46)$$

Hereafter, we do not mention whether the operation is discrete or continuous except it should be in necessity.

Given two CPTP maps \mathcal{E}_1 and \mathcal{E}_2 , their product is defined as composition,

$$(\mathcal{E}_2 \circ \mathcal{E}_1)(\hat{\rho}) \equiv \mathcal{E}_2(\mathcal{E}_1(\hat{\rho})). \quad (47)$$

This product is associative,

$$\mathcal{E}_3 \circ (\mathcal{E}_2 \circ \mathcal{E}_1) = (\mathcal{E}_3 \circ \mathcal{E}_2) \circ \mathcal{E}_1, \quad (48)$$

and closed on the space of CPTP maps. In general, CPTP maps are not invertible, so the resulting structure is a semigroup rather than a group. The product of the two CPTP map is represented with the Kraus operators as

$$\mathcal{E}_1(\hat{\rho}) = \sum_a \hat{K}_a \hat{\rho} \hat{K}_a^\dagger, \quad \mathcal{E}_2(\hat{\rho}) = \sum_b \hat{L}_b \hat{\rho} \hat{L}_b^\dagger, \quad (49)$$

then their product is

$$(\mathcal{E}_2 \circ \mathcal{E}_1)(\hat{\rho}) = \sum_{a,b} (\hat{L}_b \hat{K}_a) \hat{\rho} (\hat{L}_b \hat{K}_a)^\dagger, \quad (50)$$

so that the composed channel has Kraus operators

$$\hat{M}_{ba} = \hat{L}_b \hat{K}_a. \quad (51)$$

For any observable \hat{O} , the action of a channel on expectation values is given by

$$\text{Tr}[\mathcal{E}(\hat{\rho}) \hat{O}] = \text{Tr}[\hat{\rho} \mathcal{E}^\dagger(\hat{O})], \quad (52)$$

where \mathcal{E}^\dagger denotes the adjoint (Heisenberg–picture) map,

$$\mathcal{E}^\dagger(\hat{O}) = \sum_a \hat{K}_a^\dagger \hat{O} \hat{K}_a. \quad (53)$$

This duality underlies the phase–space representation of channels used in subsequent sections.

1. Deterministic PSF

First we take care of the effect of the image blurring with the quasi-stationary PSF as

$$\psi_O(\boldsymbol{\theta}) = \int d^2\boldsymbol{\theta}^I K_{\text{PSF}}(\boldsymbol{\theta} - \boldsymbol{\theta}^I) \psi_I(\boldsymbol{\theta}^I). \quad (54)$$

By changing the variables for the integration (see the direct derivation in App. C), we represent the observed Wigner function as

$$\begin{aligned} W_O(\boldsymbol{\theta}, \mathbf{p}) &\equiv \frac{1}{(2\pi\lambda)^2} \int d^2\boldsymbol{\xi} \psi_O(\boldsymbol{\theta} + \boldsymbol{\xi}/2) \psi_O^*(\boldsymbol{\theta} - \boldsymbol{\xi}/2) e^{-\frac{i\mathbf{p}\cdot\boldsymbol{\xi}}{\lambda}} \\ &= \int d^2\boldsymbol{\theta}^I \Pi_{\text{PSF}}(\boldsymbol{\theta} - \boldsymbol{\theta}^I, \mathbf{p}^I) W_I(\boldsymbol{\theta}^I, \mathbf{p}^I), \end{aligned} \quad (55)$$

where

$$\begin{aligned} \Pi_{\text{PSF}}(\boldsymbol{\theta}, \mathbf{p}) &= \int d^2\boldsymbol{\xi} K_{\text{PSF}}(\boldsymbol{\theta} + \boldsymbol{\xi}/2) K_{\text{PSF}}^*(\boldsymbol{\theta} - \boldsymbol{\xi}/2) e^{-\frac{i\mathbf{p}\cdot\boldsymbol{\xi}}{\lambda}}, \\ W_I(\boldsymbol{\theta}, \mathbf{p}) &\equiv \frac{1}{(2\pi\lambda)^2} \int d^2\boldsymbol{\xi} \psi_I(\boldsymbol{\theta} + \boldsymbol{\xi}/2) \psi_I^*(\boldsymbol{\theta} - \boldsymbol{\xi}/2) e^{-\frac{i\mathbf{p}\cdot\boldsymbol{\xi}}{\lambda}}. \end{aligned} \quad (56)$$

Note that in Eq. (55) the translational invariance of the point spread function preserves. One can express Eq. (55) algebraically in terms of a channel interaction

$$\begin{aligned} \hat{\rho}_O &= \mathcal{E}_{\text{PSF}}(\hat{\rho}_I), \\ \mathcal{E}_{\text{PSF}}(\hat{\rho}_I) &= \int d\mu \hat{K}(z) \hat{\rho}_I \hat{K}(z)^\dagger. \end{aligned} \quad (57)$$

Note that a channel described by a continuous Kraus operator $\hat{K}(z) = \sqrt{\Pi_{\text{PSF}}} \hat{D}(\boldsymbol{\theta}, \mathbf{0})$. Then we represent

$$W_O = \text{Tr}[\hat{\rho}_O \hat{w}] = \int d\mu \text{Tr}[\hat{K}(z) \hat{\rho}_I \hat{K}(z)^\dagger \hat{w}] \quad (58)$$

Provided a Gaussian PSF as

$$K_{\text{PSF}}(\boldsymbol{\theta}) = \frac{e^{-\frac{|\boldsymbol{\theta}|^2}{2\sigma_\theta^2}}}{2\pi\sigma_\theta^2}, \quad (59)$$

we obtain

$$\Pi_{\text{PSF}}(\boldsymbol{\theta}, \mathbf{p}) = \frac{1}{\pi\sigma_\theta^2} \exp\left(-\frac{|\boldsymbol{\theta}|^2}{\sigma_\theta^2} - \frac{\sigma_\theta^2|\mathbf{p}|^2}{\lambda^2}\right). \quad (60)$$

As we will argue in Sec. V B, Eq. (60) explicitly gives that an uncertainty relation $\lambda = \sigma_\theta \sigma_p$ where $\sigma_p = \lambda/\sigma_\theta$ ⁷, given that it is consistent to the other uncertainty relations.

2. Stochastic PSF

We describe the other extreme case that a galaxy image is blurred by a non-stationary PSF in position space, resulting in stochastic displacements of the image structure by a certain probability $\Pi_{\text{PSF}}(\Delta)$. In this case, we obtain the PSF operation as

$$\mathcal{E}_{\text{PSF}}(\hat{\rho}) = \int d^2\Delta \Pi_{\text{PSF}}(\Delta) \hat{T}(\Delta) \hat{\rho} \hat{T}^\dagger(\Delta), \quad (61)$$

where \hat{T} denotes the translation operator. Then the Wigner function is obtained as

$$W_O(\boldsymbol{\theta}, \mathbf{p}) = \int d^2\Delta \Pi_{\text{PSF}}(\Delta) W_I(\boldsymbol{\theta} - \Delta, \mathbf{p}). \quad (62)$$

We can choose a Gaussian distribution function for $\Pi_{\text{PSF}}(\Delta)$ as one of the simplest choices. We find that the deterministic PSF create a momentum coherence on the Wigner function of the source image, which reflects the fact that the PSF is stationary over the galaxy image. Such coherence is absent in the stochastic PSF as the source image is locally blurred at random, imprinting incoherent pattern on the source Wigner function. In Sec. II C, we argue how the PSF mixes the morphology and the rotational pattern of a galaxy image, featuring that the two PSFs work in such destruction in different ways.

Let us remark what is relevant to our study. We make use of the feature that the Wigner function is real but not everywhere positive; unlike a probability density, an intensity map, or a Fourier power spectrum, it shows sign-oscillations and structured zero sets that encode interference at the phase–space resolution scale set by λ . For a galaxy image field $\psi(\boldsymbol{\theta})$, the associated Wigner function $W[\psi]$ inherits these features and thus carries information beyond the intensity or Fourier power spectrum,

⁷ In this paper, we have yet to be strict in following the uncertainty relations in quantum mechanics cf. [60–62]. We would rather simply argue that the Wigner function follows an uncertainty relation as shown here and Sec. V B

however its four-dimensional nature makes direct analysis cumbersome. We therefore introduce *Wigner Function Shapelets*: an $Sp(4, \mathbb{R})$ -covariant decomposition organised by the $SU(2)$ irreducible representation of the two-mode oscillator. The procedure to make the analytic form of the (cross-)Wigner function with the mode functions are well-controlled by the linear metaplectic transformation given by the Wigner d -matrix. In the rest of the paper, we assume that the image is static in observational time in the single colour band and consider only the intensity without making use of any polarisation for simplicity. Despite such simplification it is already sufficient to show how the Wigner function captures the information of a galaxy image, which is novel in the astrophysical literature.

III. WIGNER FUNCTION SHAPELETS

In this section we construct the Wigner Function Shapelets (WFS), which is one of the main results of this paper. In the former half of this section, we define the Wigner Function Shapelets following R. Simon and G. S. Agarwal 2000 [32]. This paper presents the analytic form of the Wigner function of the LG modes. We extend their computation to cross-Wigner function via the Hopf spinor (or the two-dimensional Schwinger harmonic oscillators). Note that we follow the normalisation of the Wigner function in [32] as shown in Eq. (2) and Eq. (16). We introduce the fundamental properties of the WFS in the following three subsections. In the first, we briefly describe the WFS as a novel basis of the phase space, introducing its orthogonal and complete nature as a Hilbert-Schmidt space. In the second, we derive the analytic forms of the WFS via $SU(2)$ algebra. We introduce a key geographical feature of the WFS: oscillation and zeros in the two-dimensional $U(1)$ -invariant space of $SU(2)$ – the harmonic energy Q_0 and the angular momentum Q_2 . Note that Q_0 and Q_2 are used in [32] as dimensionless quantities. At the last, we introduce a mathematical procedure that embeds the phase space into $SU(2)$ quadrants, making use of the Hopf fibration[39]. This procedure makes WFS a unique quantity to capture the phase space structure in a symmetry-preserving manner. The physical dimensions are then defined by a typical size of the image in angular scale σ and the discretisation scale λ . We will discuss how to determine σ and λ in practical image analysis in Sec. V. Throughout this section, we omit the arguments of the functions for simple presentation unless we need to show them explicitly. Also we do not show the derivation of the Wigner function, suggesting readers to see [32].

A. Definition of Wigner Function Shapelets

Shortly speaking, the WFS is the cross-Wigner function Eq. (16) between the two LG modes $\Psi_{j,s}^{\text{LG}}$ and $\Psi_{j',s'}^{\text{LG}}$, namely $W_{(j,s),(j',s')}^{\text{LG}}$. At the polar coordinate

$\boldsymbol{\theta} = (|\boldsymbol{\theta}| \cos(\varphi), |\boldsymbol{\theta}| \sin(\varphi))$, the LG modes are defined as

$$\begin{aligned} \Psi_{j,s}^{\text{LG}}(|\boldsymbol{\theta}|, \varphi; \sigma) &= \mathcal{N}_{j,s} \left(\frac{2|\boldsymbol{\theta}|^2}{\sigma^2} \right)^{|s|} \\ &\times L_{j-|s|}^{2|s|} \left(\frac{2|\boldsymbol{\theta}|^2}{\sigma^2} \right) e^{-\frac{|\boldsymbol{\theta}|^2}{\sigma^2}} e^{i2s\varphi}, \\ \mathcal{N}_{j,s} &= \sqrt{\frac{2}{\pi \sigma^2}} \left[\frac{(j-|s|)!}{(j+|s|)!} \right]^{1/2}. \end{aligned} \quad (63)$$

Note that the LG modes are normalised as $\langle \Psi_{j,s}^{\text{LG}} | \Psi_{j',s'}^{\text{LG}} \rangle = \delta_{jj'} \delta_{ss'}$, respectively. The Fourier transform of the LG modes have self-similar expression as $\sigma \mapsto 2/\sigma$, up to a phase depending only on the total order $2j$:

$$\tilde{\Psi}_{j,s}^{\text{LG}}(|\mathbf{k}|, \varphi_{\mathbf{k}}; \sigma) = \pi \sigma^2 (-i)^{2j} \Psi_{j,s}^{\text{LG}}(|\mathbf{k}|, \varphi_{\mathbf{k}}; \frac{2}{\sigma}). \quad (64)$$

As it immediately follows, introducing the orthogonality of $\Psi_{j,s}^{\text{LG}}$ into the Moyal/Plancherel identity Eq. (21) gives that the set of $W_{(j,s),(j',s')}^{\text{LG}}$ makes an orthogonal and complete set of functions. This is our starting point, where the WFS is well-defined to decompose the Wigner function of a galaxy image in the phase space. Note that this orthogonality and completeness of the set of $W_{(j,s),(j',s')}^{\text{LG}}$ is a realisation of a Hilbert-Schmidt space as

$$\langle W_{(j_1,s_1),(j_2,s_2)}^{\text{LG}} | W_{(j_3,s_3),(j_4,s_4)}^{\text{LG}} \rangle_{\text{HS}} = \frac{\delta_{j_1 j_3} \delta_{s_1 s_3} \delta_{j_2 j_4} \delta_{s_2 s_4}}{(2\pi\lambda)^2}. \quad (65)$$

Thanks to this orthogonality, we can represent any function in the phase space that is quadratically integrable as a complete form of series expansion of WFS. In particular, the Wigner function W is expanded as

$$W = \sum_{(j,s),(j',s')} c_{(j,s),(j',s')} W_{(j,s),(j',s')}. \quad (66)$$

where

$$c_{(j,s),(j',s')} \equiv (2\pi\lambda)^2 \langle W_{(j,s),(j',s')} | W \rangle_{\text{HS}} \quad (67)$$

The series expansion Eq. (66) is mathematically related to the conventional polar shapelets [1] as follows. Let us expand the field ψ in terms of the LG modes

$$\psi = \sum_{j,s} \psi_{j,s} \Psi_{j,s}^{\text{LG}}. \quad (68)$$

Note that the reality condition of the image requires $\psi_{j,-s} = \psi_{j,s}^*$ thanks to the relation $\Psi_{j,-s}^{\text{LG}} = \Psi_{j,s}^{\text{LG}*}$. Subtracting Eq. (68) in the definition of the Wigner function Eq. (2), we find that the relation

$$c_{(j,s),(j',s')} = \psi_{j,s} \psi_{j',s'}^*, \quad (69)$$

which is nothing but the consequence of the identity Eq. (21). The coefficients are positive when $j = j'$ and $s = s'$, which is consistent with the fact that the diagonal elements of the state exhibit the probability distribution in modes. In practice, the Wigner function of a single galaxy image is real, and thus the coefficient is Hermite. One can extend these formulae in multiple types of fields as discussed in Sec. II A, which we leave as future work.

B. Closed analytic form of WFS

The WFS have the closed analytic form as a function of the phase space, which enables us to investigate the structure of the phase space rigorously. In particular, given $j = j'$ and $s = s'$, which is nothing but the Wigner function of a single LG mode, carries $U(1) \times U(1)$ invariance as it only depends on the pair of $U(1)$ -invariant variables (Q_0, Q_2) . In what follows, we review [32] that derives the Wigner function of the single LG modes, adding the extra derivation of the cross-Wigner function with the Hopf spinor that consists of the two-dimensional bosonic harmonic oscillators[63, 64]. In this paper, being aware of that we are working in angular coordinates, we employ the notation (θ, \mathbf{p}) that is different from what [32] describe while the contents are equivalent.

Let us start with $SU(2)$ algebra. Given the definition of commutation relations Eq. (3) there is $SU(2)$ algebra in quadratic forms of $\hat{\theta}_i$ and \hat{p}_i as

$$[\hat{T}_a, \hat{T}_b] = i \epsilon_{abc} \hat{T}_c, \quad [\hat{T}_a, \hat{T}_0] = 0, \quad (70)$$

with $a, b, c \in \{1, 2, 3\}$ and the Levi-Civita tensor ϵ_{abc} with $\epsilon_{123} = 1$.

$$\hat{T}_0 = \frac{1}{4\lambda} \left[\alpha^{-1} (\hat{\theta}_x^2 + \hat{\theta}_y^2) + \alpha (\hat{p}_x^2 + \hat{p}_y^2) \right] - \frac{1}{2}, \quad (71)$$

$$\hat{T}_3 = \frac{1}{4\lambda} \left[\alpha^{-1} (\hat{\theta}_x^2 - \hat{\theta}_y^2) + \alpha (\hat{p}_x^2 - \hat{p}_y^2) \right], \quad (72)$$

$$\hat{T}_1 = \frac{1}{2\lambda} \left[\alpha^{-1} \hat{\theta}_x \hat{\theta}_y + \alpha \hat{p}_x \hat{p}_y \right], \quad (73)$$

$$\hat{T}_2 = \frac{1}{2\lambda} \left(\hat{\theta}_x \hat{p}_y - \hat{\theta}_y \hat{p}_x \right), \quad (74)$$

where $\alpha = \sigma^2/2\lambda$. There are scalar variables corresponding to the operators as

$$Q_0 = \frac{1}{2} \left(\frac{\theta_x^2 + \theta_y^2}{\sigma^2} + \frac{\sigma^2 (p_x^2 + p_y^2)}{4\lambda^2} \right), \quad (75)$$

$$Q_1 = \frac{\theta_x \theta_y}{\sigma^2} + \frac{\sigma^2 p_x p_y}{4\lambda^2}, \quad (76)$$

$$Q_2 = \frac{\theta_x p_y - \theta_y p_x}{2\lambda}, \quad (77)$$

$$Q_3 = \frac{1}{2} \left(\frac{\theta_x^2 - \theta_y^2}{\sigma^2} + \frac{\sigma^2 (p_x^2 - p_y^2)}{4\lambda^2} \right). \quad (78)$$

Q_a satisfies the quadratic relations $Q_0^2 = Q_1^2 + Q_2^2 + Q_3^2$ where Q_0 represents a Casimiar constant that is invariant in any $SU(2)$ transformation. In addition to this feature, Q_0 and Q_2 carry the invariance with the linear symplectic transform.

Let us introduce dimensionless phase-space variables $\tilde{\theta} \equiv \theta/\sigma$ and $\tilde{\mathbf{p}} \equiv \sigma \mathbf{p}/(2\lambda)$. Then we introduce the two complex variables (u, v) induced from $(\tilde{\theta}, \tilde{\mathbf{p}})$ as

$$u = \frac{\tilde{\theta}^* + i\tilde{p}^*}{\sqrt{2}}, \quad v = \frac{\tilde{\theta} + i\tilde{p}}{\sqrt{2}}, \quad (79)$$

where $\tilde{\theta} = \tilde{\theta}_x + i\tilde{\theta}_y$ and $\tilde{\mathbf{p}} = \tilde{p}_x + i\tilde{p}_y$. Then we define the Hopf spinor as

$$z \equiv \begin{pmatrix} u \\ v \end{pmatrix} \in \mathbb{C}^2. \quad (80)$$

such that the Casimiar variables $Q_{0,1,2,3}$ is expressed by Pauli matrices σ_i as

$$Q_0 = \frac{z^\dagger z}{2} = \frac{|u|^2 + |v|^2}{2}, \quad (81)$$

$$Q_2 = \frac{z^\dagger \sigma_3 z}{2} = \frac{|u|^2 - |v|^2}{2}, \quad (82)$$

$$Q_3 = \frac{1}{2} z^\dagger \sigma_1 z = \Re(u^* v), \quad (83)$$

$$Q_1 = \frac{1}{2} z^\dagger \sigma_2 z = \Im(u^* v). \quad (84)$$

Hence the radii of the two circular modes are fixed by

$$|u|^2 = Q_0 + Q_2, \quad |v|^2 = Q_0 - Q_2. \quad (85)$$

For fixed (Q_0, Q_2) with $Q_0 > 0$ and $|Q_2| < Q_0$, the remaining degrees of freedom are two angular phases $(\phi_u, \phi_v) \in [0, 2\pi)^2$ defined by

$$u = \sqrt{Q_0 + Q_2} e^{i\phi_u}, \quad v = \sqrt{Q_0 - Q_2} e^{i\phi_v}. \quad (86)$$

At the operator level, the $SU(2) \oplus U(1)$ generators \hat{T}_a ($a = 1, 2, 3$) and \hat{T}_0 can be realised by two bosonic modes (the Schwinger construction). In particular, one may choose the commuting pair

$$\hat{T}_0 \pm \hat{T}_2 \propto \hat{N}_u, \hat{N}_v, \quad [\hat{N}_u, \hat{N}_v] = 0, \quad (87)$$

where $\hat{N}_u = \hat{a}_u^\dagger \hat{a}_u$ and $\hat{N}_v = \hat{a}_v^\dagger \hat{a}_v$ are the number operators of the two circular modes associated with the complex coordinates u and v . Note that $(\hat{a}_u, \hat{a}_u^\dagger)$ and $(\hat{a}_v, \hat{a}_v^\dagger)$ are related to the original operators for the canonical coordinates $\hat{\theta}_x, \hat{\theta}_y, \hat{p}_x, \hat{p}_y$ as

$$\hat{\theta}_x + \alpha \hat{p}_y = \frac{\sigma}{\sqrt{2}} (\hat{a}_u + \hat{a}_u^\dagger), \quad (88)$$

$$\hat{p}_x - \alpha^{-1} \hat{\theta}_y = \frac{\sqrt{2}\lambda}{i\sigma} (\hat{a}_u - \hat{a}_u^\dagger), \quad (89)$$

$$\hat{\theta}_x - \alpha \hat{p}_y = \frac{\sigma}{\sqrt{2}} (\hat{a}_v + \hat{a}_v^\dagger), \quad (90)$$

$$\hat{p}_x + \alpha^{-1} \hat{\theta}_y = \frac{\sqrt{2}\lambda}{i\sigma} (\hat{a}_v - \hat{a}_v^\dagger). \quad (91)$$

Consequently, the LG modes at fixed j are simultaneous eigenstates of (\hat{N}_u, \hat{N}_v) and can be labelled as

$$|\Psi_{j,s}^{\text{LG}}\rangle \equiv |n_u\rangle \otimes |n_v\rangle, \quad n_u \equiv j+s, \quad n_v \equiv j-s, \quad (92)$$

(and similarly $n'_u = j' + s'$, $n'_v = j' - s'$ for $|\Psi_{j',s'}^{\text{LG}}\rangle$). Recalling that the eigenfunctions for $|n_u\rangle$ and $|n_v\rangle$ are nothing but the Hermite-Gaussian function labelled by n_u

and n_v , respectively, we obtain the one-to-one correspondence of $\Psi_{j,s}^{\text{LG}} \rightarrow \Psi_{n_u n_v}^{\text{HG}}$. This algebraic identification is the foundation of the Hopf–spinor factorisation of phase-space objects built from LG modes. In the Hopf variables (u, v) in Eq. (80), the phase-space point is equivalently parametrised by $(Q_0, Q_2; \phi_u, \phi_v)$ at fixed (Q_0, Q_2) on the Hopf torus. Because LG modes are product Fock states in the circular basis, the two-mode Wigner kernel factorises into a tensor product of one-mode kernels. Equivalently, the cross-Wigner function factorises into a product of two one-mode cross-Wigners, one for the u mode and one for the v mode:

$$W[\Psi_{j,s}^{\text{LG}}, \Psi_{j',s'}^{\text{LG}}](u, v) = W_{n_u n'_u}^{(1)}(u) W_{n_v n'_v}^{(1)}(v), \quad (93)$$

with $n_u = j + s$, $n_v = j - s$ and $n'_u = j' + s'$, $n'_v = j' - s'$. Note none of n_u, n'_u, n_v, n'_v is negative due to the constraint $-j \leq s \leq j$ and $-j' \leq s' \leq j'$. A convenient closed form for the one-mode cross-Wigner between number states $|n_u\rangle$ and $|n_v\rangle$ is

$$\begin{aligned} W_{nn'}^{(1)}(w) &= e^{i(n-n')\phi} R_{nn'}^{(1)}(|w|) \\ R_{nn'}^{(1)}(|w|) &= \frac{(-1)^{n_<}}{\pi\lambda} \sqrt{\frac{n_<!}{n_>!}} (\sqrt{2}|w|)^{|n-n'|} \\ &\times e^{-2|w|^2} L_{n_<}^{(|n-n'|)}(4|w|^2), \end{aligned} \quad (94)$$

where $n_< \equiv \min(n, n')$ and $n_> \equiv \max(n, n')$. Note that $R_{nn'}^{(1)} = R_{n'n}^{(1)}$. Applying Eq. (94) to $w = u$ and $w = v$ and using $|u|^2 = Q_0 + Q_2$, $|v|^2 = Q_0 - Q_2$ yields the explicit closed form

$$\begin{aligned} W[\Psi_{j,s}^{\text{LG}}, \Psi_{j',s'}^{\text{LG}}](Q_0, Q_2; \phi_u, \phi_v) &= \frac{(-1)^{n_u < + n_v <}}{\pi^2 \lambda^2} \sqrt{\frac{n_u <! n_v <!}{n_u >! n_v >!}} (\sqrt{2}|u|)^{|\Delta_u|} (\sqrt{2}|v|)^{|\Delta_v|} \\ &\times e^{-2(|u|^2 + |v|^2)} e^{i(\Delta_u \phi_u + \Delta_v \phi_v)} \\ &\times L_{n_u <}^{(|\Delta_u|)}(4|u|^2) L_{n_v <}^{(|\Delta_v|)}(4|v|^2), \end{aligned} \quad (95)$$

with the “charges”

$$\begin{aligned} \Delta_u &\equiv n_u - n'_u = (j + s) - (j' + s'), \\ \Delta_v &\equiv n_v - n'_v = (j - s) - (j' - s'). \end{aligned} \quad (96)$$

Eq. (95) makes it manifest that the dependence on the Hopf-torus angles (ϕ_u, ϕ_v) is a single torus harmonic, while the remaining dependence is purely radial through $(Q_0 \pm Q_2)$. Note that this derivation extends the original derivation in [32] of the Wigner function of the single LG modes to the cross-Wigner function of the LG modes. The diagonal case $j = j'$ and $s = s'$ gives $\Delta_u = \Delta_v = 0$ and collapses to the well-known torus-invariant Wigner function (product of ordinary Laguerre polynomials) [32].

C. Hopf fibration of Wigner function

We introduce a representation of the phase-space coordinate $(\boldsymbol{\theta}, \mathbf{p})$ via the SU(2)-invariant subspace labeled by the a pair of $U(1)$ invariants (Q_0, Q_2) , i.e., energy and angular momentum. We construct a compact band map that preserves the essential symplectic content while encapsulating the full four-dimensional information. This band structure exposes the sign-alternating oscillations and the web of zeros (interference) of the Wigner function $W(\boldsymbol{\theta}, \mathbf{p})$, and we use it in the next section to construct morphology diagnostics directly from the (Q_0, Q_2) map.

The pair (ϕ_u, ϕ_v) therefore parametrises an invariant two-torus $T_{Q_0, Q_2} \simeq U(1) \times U(1)$, i.e., a Hopf torus, embedded in the normalised phase space. Given the coordinate with the Hopf spinor z , we obtain several properties of the Hopf torus as follows:

Disjointness (foliation by tori). For $(Q_0, Q_2) \neq (Q'_0, Q'_2)$,

$$T_{Q_0, Q_2} \cap T_{Q'_0, Q'_2} = \emptyset, \quad (97)$$

since a point $z \in \mathbb{C}^2$ cannot satisfy two distinct sets of level-set conditions for $(|u|^2, |v|^2)$.

Torus harmonics as $U(1)$ gauge modes. On T_{Q_0, Q_2} the residual symmetry is $U(1) \times U(1)$ acting as $(\phi_u, \phi_v) \mapsto (\phi_u + \alpha, \phi_v + \beta)$. The corresponding characters (torus harmonics) are

$$\chi_{k\ell}(\phi_u, \phi_v) = e^{i(k\phi_u + \ell\phi_v)}, \quad k, \ell \in \mathbb{Z}. \quad (98)$$

Along the Hopf fibre ($\alpha = \beta$), $\chi_{k\ell}$ carries a gauge charge $k + \ell$; the diagonal sector $k + \ell = 0$ is fibre-invariant and probes base (shape) structure at fixed (Q_0, Q_2) , while $k + \ell \neq 0$ resolves coherence along the fibre.

Averaging on the Hopf torus. Let $d\sigma$ denote the induced area element on T_{Q_0, Q_2} . The natural normalised average of a function f over the torus is

$$\langle f \rangle_{T_{Q_0, Q_2}} := 2 \int_0^{2\pi} \frac{d\phi_u}{2\pi} \int_0^{2\pi} \frac{d\phi_v}{2\pi} f, \quad (99)$$

so that $\langle 1 \rangle_{T_{Q_0, Q_2}} = 2$. Since the level sets of (Q_0, Q_2) are precisely the Hopf tori T_{Q_0, Q_2} , the coarea formula yields

$$\int_{\mathbb{R}^4} f \, d\mu(\boldsymbol{\theta}, \mathbf{p}) = (2\pi\lambda)^2 \int_0^\infty dQ_0 \int_{-Q_0}^{+Q_0} dQ_2 \langle f \rangle_{T_{Q_0, Q_2}}. \quad (100)$$

Then we define the Wigner-torus coefficients labelled by (k, ℓ) as

$$\mathcal{W}_{k\ell}(Q_0, Q_2) = \frac{1}{2} \langle W \chi_{k\ell}^* \rangle_{T_{Q_0, Q_2}}. \quad (101)$$

In particular, $\mathcal{W}_{00}(Q_0, Q_2) = \langle W \rangle_{T_{Q_0, Q_2}}$ and this obeys the normalisation rule

$$\begin{aligned} 1 &= \int_{\mathbb{R}^4} W \, d\mu(\boldsymbol{\theta}, \mathbf{p}), \\ &= (2\pi\lambda)^2 \int_0^\infty dQ_0 \int_{-Q_0}^{+Q_0} dQ_2 \mathcal{W}_{00}(Q_0, Q_2), \end{aligned} \quad (102)$$

namely, the Wigner function is the torus zero-mode. On each Hopf torus, there is a series expansion of the Wigner function as

$$W(Q_0, Q_2, \phi_u, \phi_v) = \sum_{k, \ell \in \mathbb{Z}} \mathcal{W}_{k\ell}(Q_0, Q_2) \chi_{k\ell}(\phi_u, \phi_v), \quad (103)$$

due to the orthogonality condition $\langle \chi_{k\ell} \chi_{k'\ell'}^* \rangle = 2\delta_{kk'}\delta_{\ell\ell'}$.

Gauge invariance of $\mathcal{W}_{k\ell}$ For fixed (Q_0, Q_2) , the phases $(\phi_u, \phi_v) \in [0, 2\pi]^2$ parametrize the Hopf torus and generate a natural $U(1) \times U(1)$ action

$$u \mapsto e^{i\alpha} u, \quad v \mapsto e^{i\beta} v, \quad (104)$$

under which (Q_0, Q_2) are invariant. Then Eq. (103) carries the phase factor $e^{i(k\alpha + \ell\beta)}$ which comes only from $\chi_{k\ell}$, leaving $\rho_{k\ell}$ invariant under arbitrary phase shifts. In the WFS, the cross-Wigner function is not invariant but transforms covariantly as a charged field on the torus:

$$W[\Psi_{j,s}^{\text{LG}}, \Psi_{j',s'}^{\text{LG}}] \mapsto e^{i(\Delta_u \alpha + \Delta_v \beta)} W[\Psi_{j,s}^{\text{LG}}, \Psi_{j',s'}^{\text{LG}}], \quad (105)$$

i.e. its “gauge charges” are (Δ_u, Δ_v) . Recalling that the cross-Wigner function of the LG modes, we obtain the selection rule and the explicit radial closed form:

$$\mathcal{W}_{k\ell;js}^{\text{LG}} = R_{j+s, j-s-k}^{(1)}(\sqrt{Q_0+Q_2}) R_{j-s, j-s-\ell}^{(1)}(\sqrt{Q_0-Q_2}). \quad (106)$$

Eqs. (106) provides an analytic closed form of the Hopf-torus observables $\mathcal{W}_{k\ell}$ in terms of associated Laguerre polynomials, with the entire gauge (angular) structure reduced to the Kronecker selection rule $(k, \ell) = (\Delta_u, \Delta_v)$. This is equivalent to the condition that (j, s) must be within the domain $-j + \max(0, k) \leq m \leq j - \max(0, \ell)$ given (k, ℓ) , which originates from the constraint $-j' \leq s' \leq j'$ and the selection rule. One must be careful that the domain is null at $j < (\max(0, k) + \max(0, \ell))/2$. Then Eq. (103) is represented as

$$W = \sum_{k, \ell \in \mathbb{Z}} \sum_{j \geq \frac{\max(0, k) + \max(0, \ell)}{2}} \left\{ \sum_{s=-j+\max(0, k)}^{j-\max(0, \ell)} c_{(j,s), (j-\frac{k+\ell}{2}, s-\frac{k-\ell}{2})} \mathcal{W}_{k\ell;js}^{\text{LG}} \chi_{k\ell} \right\}. \quad (107)$$

In Fig. 1, we plot the first eighty-one combinations of the WFS in Eq. (107). We find that the simultaneous flip: $n_u \mapsto n_v$ and $n'_u \mapsto n'_v$ provides the flip $Q_2 \mapsto -Q_2$, exhibiting the chiral symmetry of the WFS.

After all, for a given pair of LG modes, a single torus harmonic carries all the gauge-covariant phase information, while $\mathcal{W}_{k\ell}$ packages it into a gauge-invariant Hopf-torus observable.

Statistical isotropy and selection rule. Statistical isotropy of the galaxy field means invariance of the Wigner function under a common physical rotation $(\theta, \mathbf{p}) \mapsto (R_\alpha \theta, R_\alpha \mathbf{p})$ with $R_\alpha \in SO(2)$. In the Hopf parametrisation this induces $\phi_u \mapsto \phi_u - \alpha$ and $\phi_v \mapsto \phi_v + \alpha$, while (Q_0, Q_2) remain invariant. Hence isotropy implies $W(Q_0, Q_2, \phi_u - \alpha, \phi_v + \alpha) = W(Q_0, Q_2, \phi_u, \phi_v)$ for all α . The torus harmonics transform as $\chi_{k\ell}(\phi_u - \alpha, \phi_v + \alpha) = \chi_{k\ell}(\phi_u, \phi_v) e^{i(\ell-k)\alpha}$, so the Wigner-torus coefficients $\mathcal{W}_{k\ell}(Q_0, Q_2) = \frac{1}{2} \langle W \chi_{k\ell}^* \rangle_{T_{Q_0, Q_2}}$ can be nonzero only if this phase is trivial for all α . Therefore statistical isotropy enforces the diagonal selection rule $\mathcal{W}_{k\ell}(Q_0, Q_2) = 0$ for $k \neq \ell$, with only the spin-neutral modes surviving; for an ensemble of statistically isotropic fields this statement holds in expectation, while individual realisations may exhibit small off-diagonal components due to cosmic variance, masking, or noise.

Parity symmetry. Parity invariance corresponds to an orientation-reversing transformation $\theta \mapsto \mathcal{P}\theta$ with $\det \mathcal{P} = -1$, under which the canonical complex variables transform as $\tilde{\theta} \mapsto -\tilde{\theta}$ and $\tilde{p} \mapsto -\tilde{p}$. With the definitions $u = (\tilde{\theta}^* + i\tilde{p}^*)/\sqrt{2}$ and $v = (\tilde{\theta} + i\tilde{p})/\sqrt{2}$, this induces $(u, v) \mapsto (-u, -v)$ and therefore $(\phi_u, \phi_v) \mapsto (\phi_u + \pi, \phi_v + \pi)$, while the invariants (Q_0, Q_2) remain unchanged. The torus harmonics transform as $\chi_{k\ell}(\phi_u + \pi, \phi_v + \pi) = \chi_{k\ell}(\phi_u, \phi_v) (-1)^{k+\ell}$, so parity invariance of the Wigner function implies

$$\mathcal{W}_{k\ell}(Q_0, Q_2) = (-1)^{k+\ell} \mathcal{W}_{k\ell}(Q_0, Q_2).$$

Hence all modes with odd $k + \ell$ must vanish, while even $k + \ell$ modes are unconstrained. When combined with statistical isotropy (which enforces $k = \ell$), only even- k diagonal components \mathcal{W}_{kk} survive, and any odd- k or off-diagonal contribution signals parity violation or residual systematics.

Chiral symmetry. Chiral (handedness-reversing) symmetry corresponds to an orientation-reversing operation in phase space that preserves the isotropic invariant Q_0 while flipping the pseudoscalar invariant Q_2 . This is equivalent to the exchange $(u, v) \mapsto (v, u)$ and hence $(\phi_u, \phi_v) \mapsto (\phi_v, \phi_u)$, while

$$Q_0 = \frac{1}{2}(|u|^2 + |v|^2) \mapsto Q_0, \quad Q_2 = \frac{1}{2}(|u|^2 - |v|^2) \mapsto -Q_2,$$

reflecting the sign flip of the pseudoscalar Q_2 . Under this transformation the torus harmonics satisfy $\chi_{k\ell}(\phi_v, \phi_u) = \chi_{\ell k}(\phi_u, \phi_v)$, so invariance of the Wigner function implies the constraint

$$\mathcal{W}_{k\ell}(Q_0, Q_2) = \mathcal{W}_{\ell k}(Q_0, -Q_2).$$

This relation provides a sharp selection rule for chiral symmetry: any antisymmetric component under $(k, \ell) \leftrightarrow (\ell, k)$ accompanied by $Q_2 \rightarrow -Q_2$ directly signals intrinsic chirality or pseudoscalar contamination in the phase-space structure.

Let us mention the edge as described by the zeros of (u, v) . (i) Boundary $|Q_2| = Q_0$. The Hopf torus

collapses to a single Hopf circle. Although $\sqrt{Q_0^2 - Q_1^2} \rightarrow 0$, the torus area shrinks at the same rate, so the coarea decomposition remains finite for integrable W . (ii) Apex $Q_0 = Q_1 = 0$. Here $u = v = 0$ and S^3 collapses to a point. This set has measure zero and does not contribute to the bounded W ; if required, \mathcal{W}_{00} may be defined by a smooth limiting procedure.

D. Morphology modes and rotation modes

Let us recall two independent charge operators using a pair of Schwinger harmonic oscillators (\hat{a}_u, \hat{a}_v) ,

$$\begin{aligned}\hat{T}_0 - \frac{1}{2}\hat{I} &\equiv \frac{1}{2}(\hat{a}_u^\dagger \hat{a}_u + \hat{a}_v^\dagger \hat{a}_v), \\ \hat{T}_2 &\equiv \frac{1}{2}(\hat{a}_u^\dagger \hat{a}_u - \hat{a}_v^\dagger \hat{a}_v),\end{aligned}\quad (108)$$

which generate two commuting $U(1)$ transformations. Their actions on the ladder operators are

$$\begin{aligned}e^{-i\alpha\hat{T}_0}\hat{a}_u e^{+i\alpha\hat{T}_0} &= e^{+i\alpha}\hat{a}_u, & e^{-i\alpha\hat{T}_0}\hat{a}_v e^{+i\alpha\hat{T}_0} &= e^{+i\alpha}\hat{a}_v, \\ e^{-i\beta\hat{T}_2}\hat{a}_u e^{+i\beta\hat{T}_2} &= e^{+i\beta}\hat{a}_u, & e^{-i\beta\hat{T}_2}\hat{a}_v e^{+i\beta\hat{T}_2} &= e^{-i\beta}\hat{a}_v.\end{aligned}\quad (109)$$

Since $[\hat{T}_0, \hat{T}_2] = 0$, the corresponding charges can be simultaneously diagonalised. The two charge modes generated by $\hat{T}_J = \exp(iJ(\phi_u + \phi_v)\hat{T}_0)$ and $\hat{T}_K = \exp(iK(\phi_u - \phi_v)\hat{T}_2)$ brings the independent charge states. We dub J ($J = 0, \pm 1, \pm 2, \dots$) and K ($K = 0, \pm 1, \pm 2, \dots$) as morphology modes and rotational modes, respectively. It is well known that the Fourier power spectrum, corresponding to the marginal of the Wigner function over configuration space, retains only even J modes while all K modes survive. This reflects the fact that the Fourier power alone does not uniquely determine the image, and that odd morphology modes require higher-order configuration-space correlations. The WFS formalism makes this structure explicit: for each mode, the morphology and rotation charges are given by $J = \Delta_u + \Delta_v$ and $K = \Delta_u - \Delta_v$.

The effect PSF blurring can be understood most transparently in the Heisenberg picture, taking into account the morphology modes and the rotational modes. Following the formulation introduced in Sec. II C, we describe the decoherence of the morphology and the rotational features of a galaxy image separately for whether the PSF is deterministic or stochastic.

1. Deterministic PSF

For a deterministic PSF acting coherently on the complex field amplitude, the forward map is a single-operator channel

$$\hat{\rho}_O = \mathcal{E}_{\text{coh}}(\hat{\rho}_I) = \hat{K} \hat{\rho}_I \hat{K}^\dagger, \quad (110)$$

where $\hat{K} = K_{\text{PSF}}(\hat{\mathbf{p}})$ is the optical transfer function (OTF) acting multiplicatively in Fourier space, equivalently, a function of the momentum operator $\hat{\mathbf{p}}$. Charge preservation is therefore controlled by commutators with \hat{K} .

The morphology generator \hat{T}_0 does not commute with \hat{K} in general,

$$[\hat{T}_0, \hat{K}] \neq 0, \quad (111)$$

reflecting the fact that coherent PSF blur induces mode coupling among different morphology charges J . For a Gaussian PSF, $\hat{K} \propto \exp(-\varepsilon \hat{\mathbf{p}}^\dagger \hat{\mathbf{p}})$, this non-commutativity is governed by pair creation and annihilation operators $\hat{a}_u \hat{a}_v$ and $\hat{a}_u^\dagger \hat{a}_v^\dagger$, and its magnitude scales with the PSF width.

By contrast, the rotation generator \hat{T}_2 is preserved iff the PSF is isotropic. Since under rotations $\hat{\mathbf{p}} \rightarrow e^{+i\beta}\hat{\mathbf{p}}$, rotational covariance requires $\hat{K} = f(\hat{\mathbf{p}}^\dagger \hat{\mathbf{p}})$, equivalently $\tilde{K}_{\text{PSF}}(\mathbf{p}) = \tilde{K}_{\text{PSF}}(|\mathbf{p}|)$. Thus,

$$[\hat{T}_2, \hat{K}] = 0 \iff \text{isotropic PSF}. \quad (112)$$

Anisotropic coherent PSFs generically mix different rotation charges K .

2. Stochastic PSF

A translationally invariant PSF corresponds to a random displacement channel,

$$\begin{aligned}\mathcal{K}(\hat{\rho}) &= \int d^2\Delta K(\Delta) \hat{T}(\Delta) \hat{\rho} \hat{T}^\dagger(\Delta) \\ \hat{T}(\Delta) &= \exp\left[-\frac{i}{\lambda}(\Delta \hat{\pi}^\dagger + \Delta^* \hat{\pi})\right],\end{aligned}\quad (113)$$

with $\hat{\pi} = \frac{i}{\sqrt{2}}(\hat{a}_u^\dagger - \hat{a}_v)$. In the Heisenberg picture,

$$\mathcal{K}^\dagger(\hat{O}) = \int d^2\Delta K(\Delta) \hat{T}^\dagger(\Delta) \hat{O} \hat{T}(\Delta). \quad (114)$$

Applying this map to the morphology generator \hat{T}_0 , one finds

$$\mathcal{K}^\dagger(\hat{T}_0) = \hat{T}_0 + \frac{\langle |\Delta|^2 \rangle_{\text{PSF}}}{2\lambda^2}, \quad (115)$$

for a centred PSF with $\langle \Delta \rangle_{\text{PSF}} = 0$. Note that $\langle A \rangle_{\text{PSF}} \equiv \int d^2\Delta K(\Delta) A(\Delta)$. Thus PSF blurring induces an effective diffusion in morphology space, leading to the suppression of large- J morphology modes. In the limit $\lambda \rightarrow 0$ with $\langle |\Delta|^2 \rangle_{\text{PSF}}/\lambda^2 \rightarrow 0$, all the morphological information becomes asymptotically recoverable.

By contrast, the rotation generator obeys

$$\mathcal{K}^\dagger(\hat{T}_2) = \hat{T}_2 \quad (116)$$

for any centred PSF. However, preservation of individual rotation modes K requires the stronger condition of rotational covariance of the kernel, $K(\Delta) = K(|\Delta|)$.

Anisotropic PSFs generically mix different K sectors, while leaving the morphology diffusion unaffected.

This separation clarifies the distinct physical roles of the two charges types: morphology modes quantify the sensitivity of image structure to translational diffusion, while rotation modes probe anisotropy. As shown in Sec. IV A and Sec. IV B, weak gravitational lensing couples these modes according to well-defined selection rules, enabling targeted estimators for parity-violating and higher-spin signals.

E. Correspondence between WFS and BiPoSHs representation

We connect the WFS to the BiPoSHs representation of the angular two-point correlation function. More specifically, we derive the analytic expression of $A_{\ell_1 \ell_2}^{LM}$ in Eq. (41) in terms of the WFS. Here in this section, a character ℓ denotes a multipole moment. Let us start with the analytic expansion of the Laguerre-Gaussian mode $\Psi_{j,s}^{\text{LG}}(\boldsymbol{\theta}; \mathbf{n}_c)$ in terms of the spherical harmonics $Y_{\ell m}(\mathbf{n})$, where the small-angle approximation leads to $\mathbf{n} = \mathbf{n}_c + \boldsymbol{\theta} + \mathcal{O}(\theta^2)$. At the small angle limit around the centroid position \mathbf{n}_c , there is the asymptotic expression of $Y_{\ell m}$ as

$$Y_{\ell m} \approx \mathcal{B}_{\ell,|m|} J_{|m|}(\tau_\ell \theta) e^{im\varphi},$$

$$\mathcal{B}_{\ell,|m|} = (-1)^{|m|} \sqrt{\frac{\tau_\ell}{2\pi}} \sqrt{\frac{(\ell + |m|)!}{(\ell - |m|)!}} \tau_\ell^{-m}, \quad (117)$$

where $J_a(x)$ is the Bessel function of a -th kind and $\tau_\ell = \ell + 1/2$. Note that the angle dependence is factorised by the exponential function and thus we have a constraint $m = 2s$ as a consequence of orthogonality. Then we

obtain the following expression

$$\Psi_{j,s}^{\text{LG}}(\boldsymbol{\theta}; \mathbf{n}_c) \approx \sum_{\ell} \psi_{\ell}^{(j,s)} B_{\ell,2|s|}^{-1} Y_{\ell,2s}(\mathbf{n}). \quad (118)$$

By using the integral identity in the radial direction (see the full derivation in App. E), the coefficient is analytically derived as

$$\psi_{\ell}^{(j,s)} = \frac{\tau_\ell (-1)^{j-|s|}}{2} \left| \Psi_{j,s}^{\text{LG}} \left(\frac{\tau_\ell \sigma}{2} \right) \right|. \quad (119)$$

We find that $\psi_{\ell}^{(j,s)}$ provide a low-pass filter that localises the multipole mode by $\ell \lesssim \sigma^{-1}$. Let us plug in Eq. (118) into Eq. (2), replacing the Wigner function response to the that of the spherical harmonics. After straightforward computation, we obtain

$$\mathcal{A}_{\ell_1 \ell_2}^{LM} = \sum_{j,s,j',s'} \langle c_{(j,s),(j',s')} \rangle_{\text{cosmo.}}$$

$$\times \psi_{\ell_1}^{(j,s)} \psi_{\ell_2}^{(j',s')} B_{\ell_1,2|s|}^{-1} B_{\ell_2,2|s'|}^{-1} \langle \ell_1 2s \ell_2 2s' | LM \rangle. \quad (120)$$

One can extend the relation Eq. (120) into a generic pair of fields $(\psi_a(\boldsymbol{\theta}), \psi_b(\boldsymbol{\theta}))$, fixing the coefficient $c_{(j,s),(j',s')}$.

F. Correspondence between WFS and FPFS

We derive the dictionary between the WFS and the FPFS [7]. The Fourier power function is expressed by the WFS expansion as

$$F(\mathbf{k}) = \sum_{(j,s),(j',s')} c_{(j,s),(j',s')}$$

$$\times \tilde{\Psi}_{j,s}^{\text{LG}}(|\mathbf{k}|, \varphi_{\mathbf{k}}; \sigma) \tilde{\Psi}_{j',s'}^{\text{LG}*}(|\mathbf{k}|, \varphi_{\mathbf{k}}; \sigma). \quad (121)$$

FPFS is defined as

$$M_{j,s} = \int d^2 \mathbf{k} F(\mathbf{k}) \tilde{\Psi}_{j,s}^{\text{LG}*}(|\mathbf{k}|, \varphi_{\mathbf{k}}; \sigma). \quad (122)$$

Inserting Eq. (121) into Eq. (122), we obtain an analytic expression

$$M_{j_1,s_1} = \pi^3 \sigma^4 \sum_{(j_2,s_2),(j_3,s_3)} \delta_{s_2-s_3-s_1,0} c_{(j_2,s_2),(j_3,s_3)} \mathcal{N}_{j_1,s_1} \mathcal{N}_{j_2,s_2} \mathcal{N}_{j_3,s_3} \left(\frac{2}{3} \right)^{1+j_1+j_2+j_3}$$

$$\times \frac{(-1)^{2j_2-(|s_1|+|s_2|+|s_3|)} \Gamma[j_1+j_2+j_3+1]}{(j_1-|s_1|)!(j_2-|s_2|)!(j_3-|s_3|)!} \times F_B^{(3)} \left[-j_1-|s_1|, -j_2-|s_2|, -j_3-|s_3|; -(j_1+j_2+j_3); \frac{3}{2}, \frac{3}{2}, \frac{3}{2} \right]. \quad (123)$$

Note that we use a concise analytic notation of the integral of the triple multiplication of the Laguerre-Gaussian mode

following Eq. (11) in [65]. Here $F_B^{(3)}$ is B -type Lauricella hypergeometric function for the three variables.

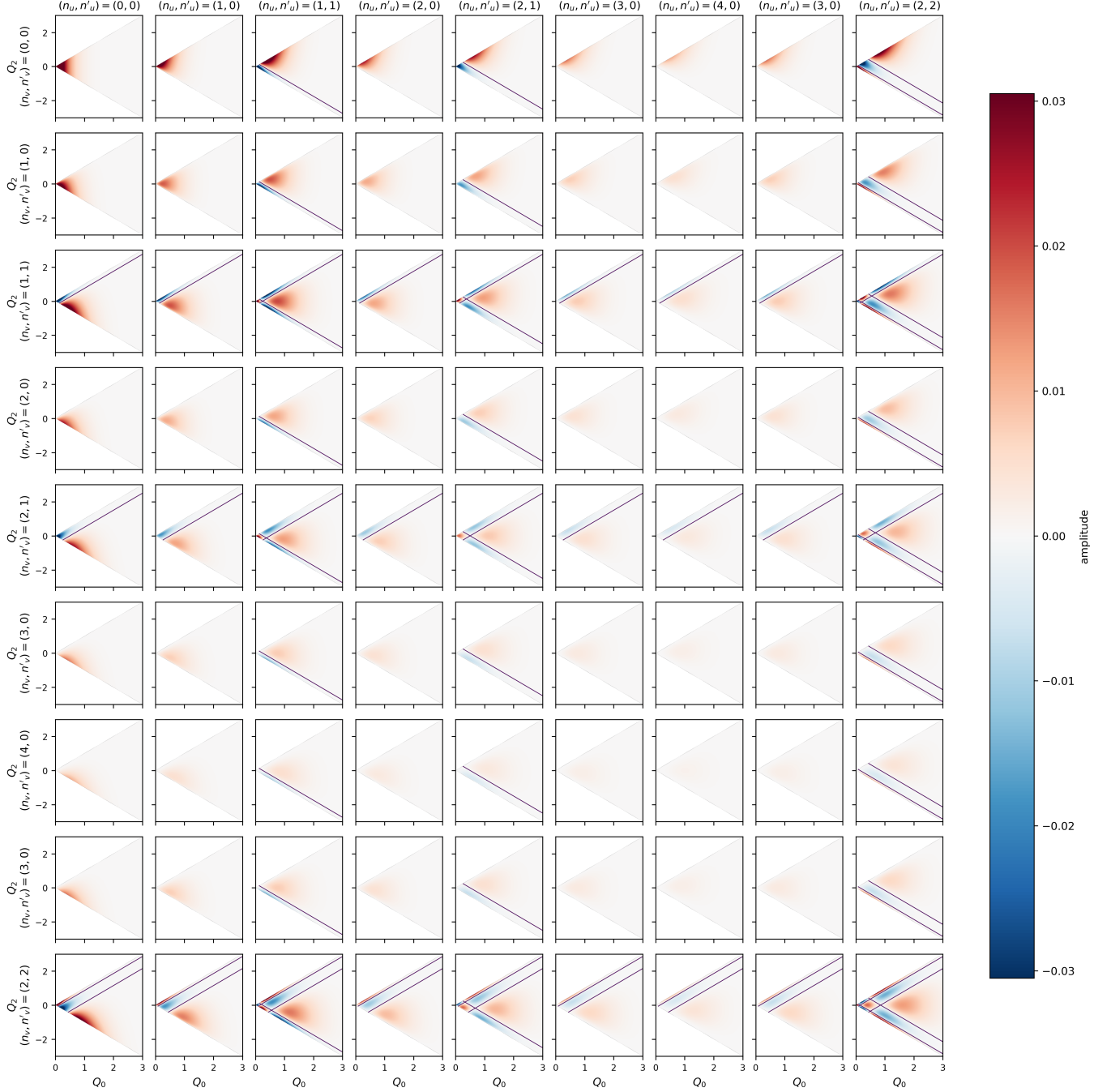


FIG. 1. Analytic band matrix in the (Q_0, Q_2) plane. Columns correspond to (n_u, n'_u) and rows to (n_v, n'_v) . Each panel shows the radial product $R_{n_u n'_u}(\sqrt{Q_0 + Q_2}) R_{n_v n'_v}(\sqrt{Q_0 - Q_2})$, masked to the physical wedge $|Q_2| \leq Q_0$.

From this expression, we find that the coefficients of the FPFS are a mixture of the fundamental modes of the image state in WFS. At the lowest modes, the expression in Eq. (123) can be simplified and it is still convenient to employ the image analysis such as shape measurements, at which the one of the lowest shear response function in the FPFS is sufficient. Given such a method of local morphology marginalisation, we employ the WFS to estimate the weak-lensing flexion and the galaxy shape statistic correlations. We will aim to show our findings in the following section. The modes in Fig. 1 are distinguished in terms of the morphological charge J and the rotational mode K . We emphasise that systematic oscillatory patterns on (Q_0, Q_2) play a critical role in characterising the phase information of the Wigner function of a galaxy image. Table. I summarises (J, K) . Note that the original modes (j, s) is recovered by

$$\begin{aligned} j &= \frac{n_u + n_v}{2}, \quad s = \frac{n_u - n_v}{2}, \\ j' &= \frac{n'_u + n'_v}{2} = j - \frac{J}{2}, \quad s' = \frac{n'_u - n'_v}{2} = s - \frac{K}{2}, \end{aligned} \quad (124)$$

TABLE I. Grouping of the 9×9 index combinations into distinct (J, K) sectors, sorted by increasing $(|J|, |K|)$. We use $k = n_u - n'_u$, $\ell = n_v - n'_v$, $J = k + \ell$, $K = k - \ell$.

J	K	k	ℓ	count	(n_u, n'_u) choices	(n_v, n'_v) choices
0	0	0	0	9	(0,0), (1,1), (2,2)	(0,0), (1,1), (2,2)
1	-1	0	1	6	(0,0), (1,1), (2,2)	(1,0), (2,1)
1	1	1	0	6	(1,0), (2,1)	(0,0), (1,1), (2,2)
2	-2	0	2	3	(0,0), (1,1), (2,2)	(2,0)
2	0	1	1	4	(1,0), (2,1)	(1,0), (2,1)
2	2	2	0	3	(2,0)	(0,0), (1,1), (2,2)
3	-3	0	3	3	(0,0), (1,1), (2,2)	(3,0)
3	-1	1	2	2	(1,0), (2,1)	(2,0)
3	1	2	1	2	(2,0)	(1,0), (2,1)
3	3	3	0	3	(3,0)	(0,0), (1,1), (2,2)
4	-4	0	4	3	(0,0), (1,1), (2,2)	(4,0)
4	-2	1	3	2	(1,0), (2,1)	(3,0)
4	0	2	2	1	(2,0)	(2,0)
4	2	3	1	2	(3,0)	(1,0), (2,1)
4	4	4	0	3	(4,0)	(0,0), (1,1), (2,2)
5	-3	1	4	2	(1,0), (2,1)	(4,0)
5	-1	2	3	1	(2,0)	(3,0)
5	1	3	2	1	(3,0)	(2,0)
5	3	4	1	2	(4,0)	(1,0), (2,1)
6	-2	2	4	1	(2,0)	(4,0)
6	0	3	3	1	(3,0)	(3,0)
6	2	4	2	1	(4,0)	(2,0)
7	-1	3	4	1	(3,0)	(4,0)
7	1	4	3	1	(4,0)	(3,0)
8	0	4	4	1	(4,0)	(4,0)

IV. COSMOLOGICAL INFORMATION IN WIGNER FUNCTION

We describe how cosmological information emerges in the Wigner function and its angular correlations. We exemplify the linear response of weak lensing i.e. shear [5] and flexions [6], cosmic birefringence[66], and higher-moment of galaxy shapes [59, 67] in the language of the Wigner function and WFS. Throughout this section, we will argue that the response function is well-defined at the local level of the image plane, implying a possibility to handle image systematics and noise at a local level. Note that we represent here the ensemble with $\langle \dots \rangle$ without mentioning the subscript that denotes the ensemble is taken over cosmological realisations.

A. Shear response

We derive the linear response to weak gravitational lensing in the Wigner function. We work in the weak-lensing regime and retain terms up to second-order of spatial derivatives of the lens potential $\Phi(\theta)$, i.e. cosmic shear, following the derivation in [68]. In the case of the shear, where the matrix $A_{ij} = \delta_{ij} + \Phi_{ij}$ ($i, j = (x, y)$)⁸ and we define the convergence $\kappa = (\Phi_{xx} + \Phi_{yy})/2$, and $\gamma = \gamma_1 + i\gamma_2 = (\Phi_{xx} - \Phi_{yy})/2 + i\Phi_{xy}$, where $\Phi_{xy} = \Phi_{yx}$. We obtain $\delta\theta = (\kappa\mathbf{I} + \boldsymbol{\Gamma})\theta^I$ and $\delta\mathbf{p} = -(\kappa\mathbf{I} + \boldsymbol{\Gamma})\mathbf{p}^I$. We shall denote the Lie derivative of the Wigner function as $\mathcal{L}_z W \equiv W^I(z) - W^S(z)$. Hereafter, we omit the superscript I for concise presentation. If we change the canonical variables to $(|u|, |v|, \phi_u, \phi_v)$, $\mathcal{L}_z W$ is rewritten as

$$\mathcal{L}_z W = -\delta|u|\partial_{|u|}W - \delta|v|\partial_{|v|}W - \delta\phi_u\partial_{\phi_u}W - \delta\phi_v\partial_{\phi_v}W, \quad (125)$$

where

$$\delta u \equiv u' - u = \gamma^* u^*, \quad \delta v \equiv v' - v = \gamma v^*. \quad (126)$$

and

$$\begin{aligned} \delta|u| &= |u|\Re(\gamma e^{2i\phi_u}), \quad \delta|v| = |v|\Re(\gamma^* e^{2i\phi_v}), \\ \delta\phi_u &= -\Im(\gamma e^{i2\phi_u}), \quad \delta\phi_v = -\Im(\gamma^* e^{i2\phi_v}). \end{aligned} \quad (127)$$

These expressions provide a complete and closed description of the linear shear response in the (u, v) variables and in the $(Q_0, Q_2, \phi_u, \phi_v)$ representation, which will be used throughout the remainder of this work.

Plugging Eqs. (126) and (127) into Eq. (125), the linear response of the weak lensing shear is derived for

⁸ We follow the convention [68], which is the inverse of the standard convention that treats A here to A^{-1} .

the observable $\mathcal{W}_{k\ell}$ as

$$\begin{aligned} \mathcal{W}_{k\ell}^I(Q_0, Q_2) - \mathcal{W}_{k\ell}^S(Q_0, Q_2) &= A_{k\ell}^\gamma \gamma + A_{k\ell}^{\gamma^*} \gamma^*, \\ A_{k\ell}^\gamma &= -\frac{1}{2} [|u|\partial_{|u|} - (k-2)] \mathcal{W}_{k-2,\ell}^S \\ &\quad - \frac{1}{2} [|v|\partial_{|v|} + (\ell+2)] \mathcal{W}_{k,\ell+2}^S, \\ A_{k\ell}^{\gamma^*} &= -\frac{1}{2} [|u|\partial_{|u|} + (k+2)] \mathcal{W}_{k+2,\ell}^S \\ &\quad - \frac{1}{2} [|v|\partial_{|v|} - (\ell-2)] \mathcal{W}_{k,\ell-2}^S. \end{aligned} \quad (128)$$

Applying the mode decomposition in terms of WFS, one may find a shear estimator with the WFS. We will leave a problem to construct a practical shear estimator in phase space in our future research.

B. Flexion response

We derive the flexion response as follows. Following the convention of the flexion as [69, 70]

$$\delta\theta = \frac{1}{4}(2\mathcal{F}|\theta|^2 + \mathcal{F}^*\theta^2 + \mathcal{G}\theta^{*2}). \quad (129)$$

We can derive the corresponding variation of the complex conjugate momentum as

$$\delta p = -\frac{\mathcal{F}}{2}(\theta p^* + \theta^* p) - \frac{\mathcal{F}^*}{2}\theta p - \frac{\mathcal{G}}{2}\theta^* p^*. \quad (130)$$

Here we denote $\mathcal{F} = [\Phi_{xxx} + \Phi_{xyy} + i(\Phi_{xxy} + \Phi_{yyy})]/2$ and $\mathcal{G} = [\Phi_{xxx} - 3\Phi_{xyy} + i(3\Phi_{xxy} - \Phi_{yyy})]/2$, where $\Phi_{xxy} = \Phi_{xyx} = \Phi_{yxx}$. With a lengthy but straightforward computation, we obtain

$$\begin{aligned} \mathcal{W}_{k\ell}^I(Q_0, Q_2) - \mathcal{W}_{k\ell}^S(Q_0, Q_2) \\ = A_{k\ell}^{\mathcal{F}}\mathcal{F} + A_{k\ell}^{\mathcal{F}^*}\mathcal{F}^* + A_{k\ell}^{\mathcal{G}}\mathcal{G} + A_{k\ell}^{\mathcal{G}^*}\mathcal{G}^*, \end{aligned} \quad (131)$$

where the coefficients are explicitly given in Eq. (F15) that we omit them for concise presentation in the main text.

C. Signals of parity violation

It has been discussed the possibility of detecting the cosmic birefringence to test the parity symmetry of the Universe [71, 72]. In the Wigner function, the birefringence appears as

$$\mathcal{W}_{k\ell}^I(Q_0, Q_2) - \mathcal{W}_{k\ell}^S(Q_0, Q_2) = \omega(k-\ell)\rho_{k\ell}^S. \quad (132)$$

One needs to take the ensemble of the source shape so that keeping the modes $k \neq \ell$ to detect the birefringence,

selecting a certain set of galaxy samples correlating with the polarised emission [72, 73].

The parity-violating feature can be inspected in terms of the shape correlation function with its trispectra [59]. We define the spin-2 parity-even and parity-odd combinations of the Hopf-projected Wigner coefficients $\rho_{k\ell}$ as

$$\begin{aligned} \mathcal{W}_{k\ell}^E &\equiv \frac{1}{2}(\mathcal{W}_{k\ell} + \mathcal{W}_{\ell k}), \\ \mathcal{W}_{k\ell}^B &\equiv \frac{1}{2i}(\mathcal{W}_{k\ell} - \mathcal{W}_{\ell k}), \quad |k-\ell|=2, \end{aligned} \quad (133)$$

where the condition $|k-\ell|=2$ selects the spin-2 sector associated with galaxy shapes. By construction, $\mathcal{W}_{k\ell}^E$ is even under parity, while $\mathcal{W}_{k\ell}^B$ is odd.

The basic parity-odd observable is the cross-correlation

$$\langle \mathcal{W}_{k\ell}^E \mathcal{W}_{k'\ell'}^{B*} \rangle = \frac{1}{4i} \langle (\mathcal{W}_{k\ell} + \mathcal{W}_{\ell k})(\mathcal{W}_{k'\ell'}^* - \mathcal{W}_{\ell'k'}^*) \rangle. \quad (134)$$

Since the Wigner function is bilinear in the galaxy image field ψ , the projected coefficient $\mathcal{W}_{k\ell}$ is itself quadratic in ψ . Consequently, the correlator in Eq. (134) is a four-point function of the underlying galaxy field,

$$\begin{aligned} \langle \mathcal{W}_{k\ell} \mathcal{W}_{k'\ell'}^* \rangle(\mathbf{n}_{c1}, \mathbf{n}_{c2}) \\ \sim \int d^2\boldsymbol{\xi}_{12} \int d^2\boldsymbol{\xi}_{34} \langle \psi(\mathbf{n}_{1+}) \psi^*(\mathbf{n}_{1-}) \psi^*(\mathbf{n}_{2+}) \psi(\mathbf{n}_{2-}) \rangle, \end{aligned} \quad (135)$$

where the four sky positions are determined by the Wigner kernels and the (k, ℓ) - (k', ℓ') projections. Therefore, $\langle \mathcal{W}_{k\ell}^E \mathcal{W}_{k'\ell'}^{B*} \rangle$ is a filtered four-point function of the galaxy field and, in harmonic space, it represents a particular projection of the angular trispectrum.

The four-point function can be decomposed into disconnected (Gaussian) and connected parts,

$$\begin{aligned} \langle \psi_{1+} \psi_{1-}^* \psi_{2+}^* \psi_{2-} \rangle &= \langle \psi_{1+} \psi_{1-}^* \rangle \langle \psi_{2+}^* \psi_{2-} \rangle + \langle \psi_{1+} \psi_{2+}^* \rangle \langle \psi_{1-}^* \psi_{2-} \rangle \\ &\quad + \langle \psi_{1+} \psi_{1-}^* \psi_{2+}^* \psi_{2-} \rangle_{\text{conn.}} \end{aligned} \quad (136)$$

For a parity-symmetric sky, the two-point functions are parity even, implying that the disconnected contribution vanishes identically in the parity-odd channel,

$$\langle \mathcal{W}_{k\ell}^E \mathcal{W}_{k'\ell'}^{B*} \rangle_{\text{disc}} = 0. \quad (137)$$

As a result, any nonzero ensemble expectation value of $\langle \mathcal{W}_{k\ell}^E \mathcal{W}_{k'\ell'}^{B*} \rangle$ must arise solely from the connected four-point function, i.e. from a parity-violating angular trispectrum.

In the limit where two galaxies are well separated on the sky, $|\mathbf{n}_{c1} - \mathbf{n}_{c2}| \gg |\boldsymbol{\theta}_{1,2}|$, this statistic probes the collapsed configuration of the trispectrum, with the centroid separation defining a large-scale multipole L . Thus, the parity-odd shape correlation constructed from $\rho_{k\ell}^E$ and $\rho_{k\ell}^B$ provides a direct and robust probe of parity violation encoded in the connected four-point statistics of the galaxy field.

D. Galaxy shape response to spin modes

We summarise a generating-functional formulation of galaxy shape moments and their spin (helicity) decomposition, formulated directly in phase space. The starting point is the image density matrix $\hat{\rho}$ and its Wigner function $W(\theta, p)$, which are in one-to-one correspondence with the Weyl characteristic function. Derivatives of χ at the origin generate phase-space moments of the state. Explicitly,

$$\frac{\partial^{n+m}\chi}{\partial\eta_{a_1}\cdots\partial\eta_{a_n}\partial\zeta_{b_1}\cdots\partial\zeta_{b_m}}\Big|_{\eta=\zeta=0} = \left(\frac{i}{\lambda}\right)^{n+m} \int d\mu W \theta_{a_1}\cdots\theta_{a_n} p_{b_1}\cdots p_{b_m}, \quad (138)$$

which correspond to Weyl-ordered (fully symmetrised) operator moments. Noting the phase-space coordinate as complex variables, we obtain

$$\partial_{\eta^*}^p \partial_{\eta}^q \partial_{\zeta^*}^r \partial_{\zeta}^s \chi \Big|_0 = \left(\frac{i}{\lambda}\right)^{p+q+r+s} \int d\mu W \theta^p(\theta^*)^q p^r(p^*)^s. \quad (139)$$

Under a physical rotation by α , $(\theta, p) \mapsto e^{i\alpha}(\theta, p)$, implying that the moment in Eq. (139) carries definite helicity

$$n = (p + r) - (q + s). \quad (140)$$

In particular, the pure configuration-space spin- n moments follow from

$$\begin{aligned} \partial_{\eta^*}^n \chi \Big|_0 &= \left(\frac{i}{\lambda}\right)^n \int d\mu W \theta^n, \\ \partial_{\eta}^n \chi \Big|_0 &= \left(\frac{i}{\lambda}\right)^n \int d\mu W (\theta^*)^n. \end{aligned} \quad (141)$$

After integrating over p , these reduce to the standard spin- n moments of the image field.

Writing the Wigner function as $W = W(|u|^2, |v|^2, \phi_u, \phi_v)$ with phase-space measure $d\mu$, it is natural to define a Hopf-spinor characteristic function by coupling sources directly to (u, v) ,

$$\chi_H(J_u, J_v) := \int d\mu W e^{J_u u + J_v v + J_u^* u^* + J_v^* v^*}. \quad (142)$$

Derivatives generate Hopf-spinor moments,

$$\partial_{J_u}^m \partial_{J_v}^n \partial_{J_u^*}^r \partial_{J_v^*}^s \chi_H \Big|_0 = \int d\mu W u^m v^n (u^*)^r (v^*)^s, \quad (143)$$

which carry torus charges $(m - r, n - s)$ under (ϕ_u, ϕ_v) shifts. The physical spin content follows from the embedding of spatial rotations into the Hopf phases in the WFS formalism.

V. PRACTICAL USAGE IN IMAGE ANALYSES

In this section, we describe how to apply the WFS in practical image analyses. We argue for a choice of the parameters σ, λ . σ plays a role in determining the typical size of a galaxy image from the data, and thus we should define σ in a data-dependent way. As for the weak gravitational lensing, we take care of the fact that σ and the lensing convergence κ cannot be disentangled from one another, which forces us to measure a reduced shear $\tilde{\gamma} = \gamma/(1 - \kappa)$. λ is relevant to the resolution of galaxy images, given the diffraction limit of a telescope/an array of interferometers or the seeing from the ground. λ is thus chosen by the property of the point spread function (PSF). We also discuss how to treat the point spread function in the framework of the WFS in terms of an algebraic notation. As we will show later, we point out that image deconvolution from the PSF can be described with operators in phase space or the reduced space of (Q_0, Q_2) .

A. Choice of σ

We introduce the two complementary ways to determine σ as follows. We introduce the second moments of the galaxy image as follows. Let θ_c be the centroid of the image intensity $I(\theta) = |\psi|^2$, and define the second moments as

$$\{\mathbf{Q}\}_{ij} = \frac{\int d^2\theta (\theta_i - \theta_{c,i})(\theta_j - \theta_{c,j})I}{\int d^2\theta I}, \quad (144)$$

The first way to determine σ is the method of the second-moment matching to a circular ground state of the LG modes, i.e., the Gaussian function $\exp[-|\theta - \theta_c|^2/\sigma^2]$. We equalise σ to the scale σ_g that is computed from the trace of the second moments as

$$\sigma = \sigma_g = \sqrt{\frac{1}{2} \text{Tr}(\mathbf{Q})}. \quad (145)$$

This definition becomes exact when the galaxy image is well approximated by a Gaussian profile. Note that this way of determining the image size has been widely used in the measurement of the cosmic shear [7, 74].

The second way to determine σ is to infer σ from the Ground-mode maximisation. Project ψ onto the orthonormal LG modes $\{\Psi_{j,s}^{\text{LG}}(\theta - \theta_c; \sigma)\}$ up to order J_{\max} . We introduce the function of σ as

$$f_{00}(\sigma) = \frac{|\psi_{00}(\sigma)|^2}{\sum_{j \leq J_{\max}} \sum_{s=-j}^j |\psi_{j,s}(\sigma)|^2}. \quad (146)$$

We choose $\sigma_* = \arg \max_{\sigma > 0} f_{00}(\sigma)$. For a nearly-Gaussian image $\sigma_* \simeq \sigma_g$, for structured morphology, σ_* adapts to concentrate power in the lowest modes, improving stability for truncated expansions. Note that we prescribe the scale cut to the image, so that the whole

analysis can compute the WFS in a stable way. To make sure of these requirements, we follow a scale cut with a top-hat selection function as

$$T(\boldsymbol{\theta}) = \begin{cases} 1 & |\boldsymbol{\theta} - \boldsymbol{\theta}_c| < r_{\text{cut}} \\ 0 & |\boldsymbol{\theta} - \boldsymbol{\theta}_c| \geq r_{\text{cut}} \end{cases} \quad (147)$$

where $r_{\text{cut}} = \alpha_{\text{cut}}\sigma_g$ (or alternatively $\alpha_{\text{cut}}\sigma_*$). In practice, $\alpha_{\text{cut}} \sim 3-5$ to one galaxy image, isolating the image field from the diffused surroundings.

B. Choice of λ

The parameter λ fixes the canonical relation between the image-plane angle $\boldsymbol{\theta}$ and its conjugate momentum \mathbf{p} . In practice, λ sets the phase-space cell area, like $(2\pi\lambda^2)$ that you regard as one resolvable unit: smaller cells overfit noise, larger cells smear morphology (spirals, bars, bulges). Most importantly, λ provides the quantisation scale of a galaxy image, where the LG eigenmodes take part, as well as the WFS. In what follows, we argue what λ should be.

Our Fourier convention is

$$\tilde{\psi}(\mathbf{k}) = \int d^2\boldsymbol{\theta} \psi(\boldsymbol{\theta}) e^{-i\mathbf{k}\cdot\boldsymbol{\theta}}, \quad \mathbf{k} = \mathbf{p}/\lambda. \quad (148)$$

Let σ_θ denote a characteristic angular resolution (e.g. PSF width) and σ_p is a characteristic half-bandwidth in \mathbf{p} -space from the optical transfer function (OTF), which is defined as the Fourier transform of the PSF as

$$K_{\text{OTF}}(\mathbf{p}/\lambda) \equiv \int d^2\boldsymbol{\theta} K_{\text{PSF}}(\boldsymbol{\theta}) e^{-\frac{i\mathbf{p}\cdot\boldsymbol{\theta}}{\lambda}}. \quad (149)$$

For a reference Gaussian, $\sigma_\theta\sigma_k = 1$ with σ_k the width of $\tilde{\psi}(\mathbf{k})$, hence $\sigma_p = \lambda\sigma_k$ and

$$\lambda = \sigma_\theta\sigma_p. \quad (150)$$

Thus matching λ to your instrument/data amounts to matching the resolution \times bandwidth product. In the absence of additional systematic blurring—such as atmospheric turbulence for ground-based telescopes—an astronomical image reaches the diffraction limit set by the finite aperture, where any astronomical images are inevitably unresolved. For a circular pupil of diameter D , the incoherent PSF is given by the Airy pattern,

$$I(\theta) \propto \left[\frac{2J_1(x)}{x} \right]^2, \quad x \equiv \frac{\pi D}{\lambda_{\text{phys}}} \theta,$$

where J_1 is the Bessel function of the first kind. The full width at half maximum (FWHM) is determined by the solution $[2J_1(x_{1/2})/x_{1/2}]^2 = 1/2$, which yields $x_{1/2} \simeq 1.6163$ and hence

$$\text{FWHM} = 2\theta_{1/2} = \frac{2x_{1/2}}{\pi} \frac{\lambda_{\text{phys}}}{D} \simeq 1.028 \frac{\lambda_{\text{phys}}}{D}.$$

Approximating the Airy core by a Gaussian of equal FWHM then gives

$$\sigma_\theta = \frac{\text{FWHM}}{2\sqrt{2\ln 2}} \simeq 0.437 \frac{\lambda_{\text{phys}}}{D}.$$

OTF of a clear circular pupil has compact support and vanishes for angular spatial frequencies larger than

$$\kappa_c \simeq \frac{2\pi D}{\lambda_{\text{phys}}},$$

so a characteristic momentum-space bandwidth may be taken as $\sigma_p \simeq \kappa_c/2 = \pi D/\lambda_{\text{phys}}$. The corresponding phase-space area is therefore

$$\lambda \equiv \sigma_\theta\sigma_p \simeq 0.437\pi \simeq 1.37 \quad (\mathcal{O}(1)), \quad (151)$$

demonstrating that a diffraction-limited image naturally occupies a phase-space cell of order unity. In real observations, however, other systematics add to the diffraction limits, making the image smoother. In what follows, we write down several systematics:

Seeing-limited. The image is further blurred by atmospheric turbulence for ground-based telescopes, reaching the seeing limit. In this case, one should take σ_θ from the measured seeing FWHM and σ_p from the empirical modulation transfer function (MTF) half-power or effective support; set $\lambda = \sigma_\theta\sigma_p$.

Radio interferometry. Radio interferometry overcomes the atmospheric seeing limit by observing at long wavelengths and by synthesising an effective aperture from widely separated antennas. In this case, however, the measured sky modes are no longer continuous: the interferometer samples the Fourier plane only at discrete baseline vectors, leading to the well-known problem of incomplete uv coverage [75, 76]. For an array with maximum projected baseline b_{max} , the synthesised beam sets the characteristic angular resolution $\sigma_\theta \sim \lambda_{\text{phys}}/b_{\text{max}}$, up to a numerical factor that depends on the detailed baseline distribution and weighting scheme. In Fourier space, the sampled visibility function has compact support bounded by the longest baseline, implying a cutoff in angular spatial frequency $\kappa_c \simeq 2\pi b_{\text{max}}/\lambda_{\text{phys}}$. A representative momentum-space bandwidth may therefore be taken as $\sigma_p \simeq \kappa_c/2$. The resulting phase-space area then satisfies

$$\lambda \equiv \sigma_\theta\sigma_p \sim \mathcal{O}(1),$$

indicating that, despite incomplete mode sampling, the synthesised image produced by a radio interferometer occupies a phase-space cell comparable to that of a diffraction-limited optical system.

Additional instrumental blurring mechanisms. Astronomical images are further degraded by several instrumental effects that suppress high-spatial-frequency modes. In Fourier space, these effects act multiplicatively on the OTF, while in the image plane, they broaden the effective PSF. To leading order, these blurs are well approximated

as Gaussian and may be combined in quadrature [76, 77]. The first one is pointing jitter. Random telescope pointing fluctuations during an exposure are well described by a Gaussian angular displacement with rms width $\sigma_{\theta,\text{jit.}}$ [78]. The resulting image is the convolution of the diffraction-limited PSF with the jitter kernel.

Secondly, the pixel response matters in image detection. Finite pixel size introduces an additional blur corresponding to the pixel response function. For square pixels of angular width p , the image is convolved with a top-hat kernel, yielding an OTF factor $K_{\text{OTF,pix.}} = \text{sinc}(\frac{\kappa_x p}{2}) \text{sinc}(\frac{\kappa_y p}{2})$, where $\text{sinc}(x) = \sin x/x$ [76]. For engineering estimates, the pixel blur is often replaced by a Gaussian with equivalent variance, $\sigma_{\theta,\text{pix.}} \approx p/\sqrt{12}$, corresponding to the second moment of a square top-hat response.

Thirdly, detector charge diffusion occurs when CCD/CMOS stores the image. In CCD and CMOS detectors, photoelectrons diffuse laterally before collection, producing an approximately Gaussian broadening of the image with rms width $\sigma_{\theta,\text{det.}}$ [79].

Treating all non-diffraction blurring mechanisms as a Gaussian in the image plane, and to add their variances in quadrature,

$$\sigma_{\theta,\text{tot.}}^2 \approx \sigma_{\theta,\text{diff.}}^2 + \sigma_{\theta,\text{jit.}}^2 + \sigma_{\theta,\text{pix.}}^2 + \sigma_{\theta,\text{det.}}^2. \quad (152)$$

This prescription defines the effective resolution element of the system and naturally identifies the minimum resolvable phase-space cell. Consequently, Wigner-space structure below this scale should not be over-interpreted as physically meaningful.

One may determine λ in a data-driven way from the image. In this case we propose to make use of

$$\sigma_{\theta}^2 = \frac{\int d^2\theta |\theta - \bar{\theta}|^2 I(\theta)}{\int d^2\theta I(\theta)}, \quad \sigma_k^2 = \frac{\int |\mathbf{k}|^2 |\tilde{\psi}(\mathbf{k})|^2 d^2\mathbf{k}}{\int |\tilde{\psi}(\mathbf{k})|^2 d^2\mathbf{k}}. \quad (153)$$

With $\mathbf{p} = \lambda \mathbf{k}$ we have $\sigma_p = \lambda \sigma_k$, hence enforce the Gaussian reference $\sigma_{\theta} \sigma_k = 1$ to get λ . With this choice, $\lambda = \mathcal{O}(1)$ at the angular scales where galaxy morphology lives, and the Wigner phase-space analysis resolves exactly what the instrument can support—no less, no more.

C. Existence of optimal recovery

In order to quantify how much morphological information is preserved under systematics and noise, we evaluate the information-theoretic fidelity of a channel on a certain ensemble of galaxy images, generalising the single image state for the moment. Let $\hat{\rho}_I$ denote the ensemble (source) state on the Hilbert space \mathcal{H}_{λ} truncated by λ , for example obtained from a population distribution $p(\psi)$ as $\hat{\rho}_I = \mathbb{E}_{\psi \sim p} [|\psi\rangle\langle\psi|]$. The observation process (PSF, diffusion, detector noise, etc.) is a CPTP map \mathcal{E} , so that $\hat{\rho}_O = \mathcal{E}(\hat{\rho}_I)$.

Let us introduce an abstract reference system R and a purification $|\Psi_{\hat{\rho}_I}\rangle \in \mathcal{H}_{\lambda} \otimes \mathcal{H}_R$ satisfying $\text{Tr}_R[|\Psi_{\hat{\rho}_I}\rangle\langle\Psi_{\hat{\rho}_I}|] = \hat{\rho}_I$. The entanglement fidelity of a channel \mathcal{N} acting on the image system is defined by

$$F_e(\hat{\rho}_I, \mathcal{N}) \equiv \langle \Psi_{\hat{\rho}_I} | (\mathcal{N} \otimes \mathbb{I}_R) (|\Psi_{\hat{\rho}_I}\rangle\langle\Psi_{\hat{\rho}_I}|) |\Psi_{\hat{\rho}_I}\rangle. \quad (154)$$

This quantity satisfies $0 \leq F_e \leq 1$ and is independent of the particular choice of purification. Operationally, F_e measures the fraction of Schumacher-compressible information of the source $\hat{\rho}_I$ that is preserved by \mathcal{N} , including all correlations encoded in off-diagonal mode coherences.

If \mathcal{N} admits a Kraus representation $\mathcal{N}(\hat{\rho}) = \sum_a \hat{K}_a \hat{\rho} \hat{K}_a^\dagger$, then the entanglement fidelity admits the useful expression

$$F_e(\hat{\rho}_I, \mathcal{N}) = \sum_a |\text{Tr}(\hat{\rho}_I \hat{K}_a)|^2. \quad (155)$$

For a continuous Kraus index z , the sum is replaced by an integral,

$$F_e(\hat{\rho}_I, \mathcal{N}) = \int d\mu(z) |\text{Tr}(\hat{\rho}_I \hat{K}(z))|^2. \quad (156)$$

A reconstruction (denoising/deconvolution) is itself a CPTP map \mathcal{R} applied to the observed state, producing a recovery of an image as

$$\hat{\rho}_{\text{rec}} = \mathcal{R}(\hat{\rho}_O). \quad (157)$$

We assess performance at the ensemble level via the entanglement fidelity of the effective channel

$$\mathcal{N} \equiv \mathcal{R} \circ \mathcal{E}, \quad F_e(\hat{\rho}_I, \mathcal{R} \circ \mathcal{E}). \quad (158)$$

Within this framework, an information-theoretically optimal denoiser is a recovery map that maximizes F_e (or an equivalent monotone) over an allowed class of physically admissible reconstructions \mathcal{R} ,

$$\mathcal{R}_* \in \arg \max_{\mathcal{R} \in \mathfrak{R}} F_e(\hat{\rho}_I, \mathcal{R} \circ \mathcal{E}). \quad (159)$$

The constraint set \mathfrak{R} may incorporate practical structure such as symmetry-equivariance, locality in mode space, or computational tractability.

The total observation channel is the composition

$$\mathcal{E} = \mathcal{E}_{\text{noise}} \circ \mathcal{E}_{\text{PSF}}, \quad \hat{\rho}_O = \mathcal{E}(\hat{\rho}_I), \quad (160)$$

which remains Gaussian and translationally invariant. In phase space, the combined kernel is again Gaussian,

$$\Pi_{\text{tot}}(\theta, p) \propto \exp(-\theta^\top \mathbf{A} \theta - p^\top \mathbf{B} p), \quad (161)$$

with covariance matrices \mathbf{A}, \mathbf{B} determined by β and the noise strengths γ_i . We expand W_I and W_K in terms of the torus harmonics as

$$W_I = \sum_{(J,K) \in \mathbb{Z}_{\text{even}}^2} \tilde{W}_{JK}(\mathbf{Q}) \tilde{\chi}_{JK}(\phi),$$

$$W_K = \sum_{(J,K) \in \mathbb{Z}_{\text{even}}^2} \tilde{\mathcal{K}}_{JK}(z; \mathbf{Q}) \tilde{\chi}_{JK}(\phi). \quad (162)$$

Here we define $\mathbb{Z}_{\text{even}}^2 \equiv \{(J, K) \in \mathbb{Z}^2 \mid J \equiv K \pmod{2}\}$, and $\tilde{\mathcal{W}}_{JK} \equiv \mathcal{W}_{\frac{J+K}{2}, \frac{J-K}{2}}$ and $\tilde{\chi}_{JK} \equiv \chi_{\frac{J+K}{2}, \frac{J-K}{2}}$. Note that we concisely denote $\mathbf{Q} = (Q_0, Q_2)$ and $\phi = (\phi_u, \phi_v)$. The label z denotes the continuous spectrum of the kernel. The entanglement fidelity can be written as a quadratic form

$$F_e = \sum_{(J, K) \in \mathbb{Z}_{\text{even}}^2} \sum_{(J', K') \in \mathbb{Z}_{\text{even}}^2} \times \int d\mathbf{Q} d\mathbf{Q}' \mathcal{W}_{JK}(\mathbf{Q}) \mathcal{M}_{JK, J'K'}(\mathbf{Q}, \mathbf{Q}') \mathcal{W}_{J'K'}^*(\mathbf{Q}'), \quad (163)$$

where we have defined the fidelity kernel as

$$\mathcal{M}_{JK, J'K'}(\mathbf{Q}, \mathbf{Q}') \equiv (2\pi)^4 \int d\mu(z) \mathcal{K}_{JK}(z; \mathbf{Q}) \mathcal{K}_{J'K'}^*(z; \mathbf{Q}'). \quad (164)$$

Let us interpret the above formulation in more detail. The kernel $\mathcal{M}_{JK, J'K'}$ is a positive semidefinite operator on the space of WFS coefficients and encodes the combined effect of the forward imaging channel and the recovery map. Its spectral properties determine which combinations of morphology and rotation charges are information-bearing and which are irretrievably lost:

- Eigenmodes of \mathcal{M} with large eigenvalues correspond to charge combinations that can be faithfully recovered.
- Small or vanishing eigenvalues signal directions in (J, K, \mathbf{Q}) -space where information is erased by PSF blurring and noise.
- The maximal achievable entanglement fidelity is obtained by restricting reconstruction to the support of \mathcal{M} .

For a stationary PSF and homogeneous noise, translational invariance ensures diagonalisation in Fourier space, while rotational covariance further constrains the kernel to be block-diagonal in the rotation charge:

$$\mathcal{M}_{JK, J'K'} \propto \delta_{KK'} \mathcal{M}_{JJ'}^{(K)}. \quad (165)$$

In this case, different K sectors are independent, and information loss is governed primarily by mixing among the morphology charges J within each rotation sector. Isotropic PSFs preserve the K labels, whereas anisotropic PSFs induce off-diagonal couplings between different J blocks. Within any symmetry-equivariant class of CPTP recovery maps \mathcal{R} , the entanglement-fidelity-optimal reconstruction corresponds to choosing \mathcal{R} such that the effective kernel \mathcal{K} is optimally inverted (with regularisation) on its support. In practice this leads to Wiener- or Petz-type [80] operators that act block-by-block in (J, K) space. The WFS basis therefore provides a natural coordinate system in which the fidelity kernel is

sparse, symmetry-adapted, and directly interpretable. The WFS decomposition does not eliminate information loss—which is fundamentally bounded by \mathcal{M} —but renders it explicit. By diagonalising the symmetry structure of \mathcal{M} , it enables recovery maps that saturate the maximum achievable entanglement fidelity while preserving all symmetry-protected morphology and rotation modes.

D. Feasibility

We describe how feasible the methodology of image analysis in terms of the WFS is, aligned with the timeline of the present and the forthcoming surveys. At the level of the data compression into the Wigner function, it should be available as it shares the same procedure as the standard Fourier transform, and the mathematics behind WFS is rigorous. What is non-trivial in the WFS is to reconstruct the image of galaxies within the framework of the quantum information theory, which few have addressed similar algorithms in practical image analysis in astronomy, except a couple of conceptual proposal for future telescopes cf. [81]. Although this may sound too futuristic, it has been rapidly developing in other area of research, such as quantum image processing [82, 83]. To this end, our methodology should be developed in astronomy, and we need to further examine how much our methodology can be advantageous the conventional image processing in astronomy.

VI. CONCLUSIONS

We have extended the conventional shapelet analysis for galaxy images into the *Wigner Function Shapelets* (WFS). The WFS decomposes the Wigner function of the galaxy image directly in the four-dimensional phase space, making the quantum information theory in image processing available. After sorting a useful extraction of the topological information of images via Hopf fibration of the phase space, we have found a useful observable $\mathcal{W}_{kl}(Q_0, Q_2)$ with the two rotational-invariant phase-space variables (Q_0, Q_2) . We have computed the linear response to the weak gravitational lensing. In addition, we have found a probe for any parity-violating signature in the ensemble average of a pair product of the Wigner function of the two galaxy images. This paper is written to provide a baseline formalism of WFS. We will validate our methodology in practical image analysis, looking into image simulations as well as real-data processing.

In astronomy, analyses of shapes of astronomical objects serve to provide physical information about astronomical systems since the pioneering observations carried out over the centuries by [84–91]. In the modern context, the range of studies has expanded to galaxy morphology [92–96], structure formation [97], as well as testing fundamental physics of gravity [98]. The higher resolution astronomical images can be obtained in many astronomi-

cal observations, cf. the Event Horizon Telescope [98], the more attention to developing shape analysis e.g. machine learning. [99, 100], while parity-violating effects can rotate polarization or induce cosmic birefringence [71, 101]. These science targets motivate estimators that are robust to intrinsic morphology, anisotropic point-spread functions (PSFs), masking, and source blending. To this end, we aim to establish the WFS as a novel way of image analyses ahead of the future, during which some of the fundamental questions in astrophysics and cosmology may be solved.

ACKNOWLEDGMENTS

SA thanks Tsutomu Takeuchi for future encouraging applications of WFS in galaxy image analysis. SA also thanks Eiichiro Komatsu and Fumihiro Naokawa for insightful discussions. SA is supported by the Japan Society for the Promotion of Science (JSPS) Grants-in-Aid for Scientific Research (KAKENHI) Grant No. JP24K17045.

Appendix A: Classical limit of Wigner function and Wigner transport

We describe how the classical Liouville equation is derived from the Wigner function and the Wigner transport at the limit of $\lambda \rightarrow 0$, where the resolution of the system is infinitesimal. Then we conclude that the Wigner function is proportional to the radiance (or specific intensity), and the Liouville equation we obtain is nothing but the radiative transfer equation of an image.

Let us assume a semiclassical family of image-plane fields of the form

$$\psi(\boldsymbol{\theta}) = a(\boldsymbol{\theta}) \exp\left[\frac{i}{\lambda} S(\boldsymbol{\theta})\right], \quad (\text{A1})$$

with smooth real phase $S(\boldsymbol{\theta})$ and slowly varying complex amplitude $a(\boldsymbol{\theta})$. In other words, we take a WKB approximation for the image field. The Wigner function is expressed by $a(\boldsymbol{\theta})$ and $S(\boldsymbol{\theta})$ as

$$W(\boldsymbol{\theta}, \mathbf{p}) = \frac{1}{(2\pi\lambda)^2} \int d^2\xi a\left(\boldsymbol{\theta} + \frac{\xi}{2}\right) a^*\left(\boldsymbol{\theta} - \frac{\xi}{2}\right) e^{\frac{i}{\lambda} \Phi(\boldsymbol{\theta}, \mathbf{p}; \xi)}, \quad (\text{A2})$$

with phase

$$\Phi(\boldsymbol{\theta}, \mathbf{p}; \xi) = S\left(\boldsymbol{\theta} + \frac{\xi}{2}\right) - S\left(\boldsymbol{\theta} - \frac{\xi}{2}\right) - \mathbf{p} \cdot \xi. \quad (\text{A3})$$

Rescale the integration variable as $\xi = \lambda \mathbf{y}$ to obtain

$$W(\boldsymbol{\theta}, \mathbf{p}) = \frac{1}{(2\pi)^2} \int d^2\mathbf{y} a\left(\boldsymbol{\theta} + \frac{\lambda}{2}\mathbf{y}\right) a^*\left(\boldsymbol{\theta} - \frac{\lambda}{2}\mathbf{y}\right) e^{i\Psi(\boldsymbol{\theta}, \mathbf{p}; \mathbf{y}, \lambda)}, \quad (\text{A4})$$

where

$$\Psi(\boldsymbol{\theta}, \mathbf{p}; \mathbf{y}, \lambda) = \frac{S(\boldsymbol{\theta} + \frac{\lambda}{2}\mathbf{y}) - S(\boldsymbol{\theta} - \frac{\lambda}{2}\mathbf{y})}{\lambda} - \mathbf{y} \cdot \mathbf{p}. \quad (\text{A5})$$

Executing Taylor expansion of λ at fixed $\boldsymbol{\theta}$ and using that the difference is odd in \mathbf{y} gives

$$\frac{S(\boldsymbol{\theta} + \frac{\lambda}{2}\mathbf{y}) - S(\boldsymbol{\theta} - \frac{\lambda}{2}\mathbf{y})}{\lambda} = \mathbf{y} \cdot \nabla_{\boldsymbol{\theta}} S(\boldsymbol{\theta}) + \mathcal{O}(\lambda^2 |\mathbf{y}|^3), \quad (\text{A6})$$

and similarly

$$a\left(\boldsymbol{\theta} \pm \frac{\lambda}{2}\mathbf{y}\right) = a(\boldsymbol{\theta}) \pm \mathcal{O}(\lambda |\mathbf{y}|). \quad (\text{A7})$$

Keeping the leading terms in phase and amplitude,

$$W(\boldsymbol{\theta}, \mathbf{p}) = \frac{1}{(2\pi)^2} \int d^2\mathbf{y} |a(\boldsymbol{\theta})|^2 e^{i\mathbf{y}(\nabla_{\boldsymbol{\theta}} S(\boldsymbol{\theta}) - \mathbf{p})} + \mathcal{O}(\lambda). \quad (\text{A8})$$

Using the Fourier identity $\frac{1}{(2\pi)^2} \int d^2\mathbf{y} e^{i\mathbf{y} \cdot \mathbf{q}} = \delta(\mathbf{q})$, we obtain the distributional limit

$$W(\boldsymbol{\theta}, \mathbf{p}) \xrightarrow{\lambda \rightarrow 0} L(\boldsymbol{\theta}, \mathbf{p}) = |a(\boldsymbol{\theta})|^2 \delta(\mathbf{p} - \nabla_{\boldsymbol{\theta}} S(\boldsymbol{\theta})). \quad (\text{A9})$$

Thus the Wigner function concentrates on the Lagrangian manifold $\{(\boldsymbol{\theta}, \mathbf{p}) : \mathbf{p} = \nabla_{\boldsymbol{\theta}} S(\boldsymbol{\theta})\}$ with weight $|a(\boldsymbol{\theta})|^2$. The limit $L(\boldsymbol{\theta}, \mathbf{p})$ is a positive Radon measure on phase space: a nonnegative generalized density (possibly singular) integrable against smooth test functions.

The measure $L(\boldsymbol{\theta}, \mathbf{p})$ is the classical radiance (or specific intensity) on the image-plane phase space: it assigns power per unit projected area per unit solid angle (per unit frequency/wavelength if spectral). In fact, its $\boldsymbol{\theta}$ -marginal recovers the image intensity:

$$\int L(\boldsymbol{\theta}, \mathbf{p}) d^2\mathbf{p} = |a(\boldsymbol{\theta})|^2 = \lim_{\lambda \rightarrow 0} |\psi(\boldsymbol{\theta})|^2 \equiv I(\boldsymbol{\theta}), \quad (\text{A10})$$

while its \mathbf{p} -marginal gives the classical distribution over propagation directions (spatial frequencies). For a finite superposition $\psi = \sum_n a_n(\boldsymbol{\theta}) \exp[iS_n(\boldsymbol{\theta})/\lambda]$ one has $W = \sum_n W_{nn} + \sum_{n \neq n'} W_{nn'}$. Each diagonal term W_{nn} converges to $|a_n(\boldsymbol{\theta})|^2 \delta(\mathbf{p} - \nabla_{\boldsymbol{\theta}} S_n(\boldsymbol{\theta}))$. The cross terms $W_{nn'}$ carry rapidly oscillating phase $\exp[i(S_n - S_{n'})/\lambda]$ and vanish in the weak limit by non-stationary-phase (unless $\nabla_{\boldsymbol{\theta}} S_n = \nabla_{\boldsymbol{\theta}} S_{n'}$ on a set of measure zero, e.g. caustics). Hence

$$W \rightharpoonup L(\boldsymbol{\theta}, \mathbf{p}) = \sum_n |a_n(\boldsymbol{\theta})|^2 \delta(\mathbf{p} - \nabla_{\boldsymbol{\theta}} S_n(\boldsymbol{\theta})), \quad (\text{A11})$$

a positive phase-space measure with no residual Wigner negativity.

If ψ evolves under a generator with Weyl symbol $H_W(\boldsymbol{\theta}, \mathbf{p})$, the exact Moyal evolution $\partial_s W = \{H_W, W\}_{\text{MB}}$ as shown in Eq. (10) reduces as $\lambda \rightarrow 0$ to the Liouville (radiative-transfer) equation

$$\partial_s L + \{H, L\}_{\text{PB}} = 0, \quad (\text{A12})$$

so radiance is transported along Hamiltonian rays. For quadratic Hamiltonian H this transport law already holds exactly for all λ . In the rest of the section, we derive that the quadratic Hamiltonian H is derived from the Wigner symbol H_W , completing the whole logic to be consistent.

Define the canonical momentum operator

$$\hat{\mathbf{p}} = -i\lambda\nabla_{\boldsymbol{\theta}}, \quad (\text{A13})$$

so that the commutators are $[\hat{\theta}_i, \hat{p}_j] = i\lambda\delta_{ij}$ (with $i, j \in \{x, y\}$). Then

$$\hat{H} = -\frac{\lambda^2}{2}\nabla_{\boldsymbol{\theta}}^2 + \hat{V} = \frac{\hat{\mathbf{p}}^2}{2} + \hat{V}, \quad (\text{A14})$$

If an operator \hat{A} has kernel $A(\boldsymbol{\theta}_1, \boldsymbol{\theta}_2)$ in the angle basis, its Weyl symbol is

$$A_W(\boldsymbol{\theta}, \mathbf{p}) = \int d^2\boldsymbol{\xi} A\left(\boldsymbol{\theta} + \frac{\boldsymbol{\xi}}{2}, \boldsymbol{\theta} - \frac{\boldsymbol{\xi}}{2}\right) e^{-\frac{i\mathbf{p}\cdot\boldsymbol{\xi}}{\lambda}}. \quad (\text{A15})$$

For $(\hat{V}f)(\boldsymbol{\theta}) = V(\boldsymbol{\theta})f(\boldsymbol{\theta})$, the kernel is $V(\boldsymbol{\theta}_1, \boldsymbol{\theta}_2) = V(\boldsymbol{\theta}_1)\delta(\boldsymbol{\theta}_1 - \boldsymbol{\theta}_2)$, hence

$$(V)_W(\boldsymbol{\theta}, \mathbf{p}) = V(\boldsymbol{\theta}) \quad (\text{exact}). \quad (\text{A16})$$

For $\hat{T} = \hat{\mathbf{p}}^2/2$, the kernel is

$$T(\boldsymbol{\theta}_1, \boldsymbol{\theta}_2) = -\frac{\lambda^2}{2}\nabla_{\boldsymbol{\theta}_1}^2\delta(\boldsymbol{\theta}_1 - \boldsymbol{\theta}_2). \quad (\text{A17})$$

Write $\boldsymbol{\theta} = \frac{1}{2}(\boldsymbol{\theta}_1 + \boldsymbol{\theta}_2)$ and $\boldsymbol{\xi} = \boldsymbol{\theta}_1 - \boldsymbol{\theta}_2$. Since δ depends only on $\boldsymbol{\xi}$, we obtain

$$T\left(\boldsymbol{\theta} + \frac{\boldsymbol{\xi}}{2}, \boldsymbol{\theta} - \frac{\boldsymbol{\xi}}{2}\right) = -\frac{\lambda^2}{2}\nabla_{\boldsymbol{\xi}}^2\delta(\boldsymbol{\xi}). \quad (\text{A18})$$

Thus

$$\begin{aligned} (T)_W(\boldsymbol{\theta}, \mathbf{p}) &= \int d^2\boldsymbol{\xi} \left[-\frac{\lambda^2}{2}\nabla_{\boldsymbol{\xi}}^2\delta(\boldsymbol{\xi}) \right] e^{-\frac{i\mathbf{p}\cdot\boldsymbol{\xi}}{\lambda}} \\ &= -\frac{\lambda^2}{2} \int d^2\boldsymbol{\xi} \delta(\boldsymbol{\xi}) \nabla_{\boldsymbol{\xi}}^2 e^{-\frac{i\mathbf{p}\cdot\boldsymbol{\xi}}{\lambda}} \\ &= \frac{\lambda^2}{2} \left[\frac{\mathbf{p}^2}{\lambda^2} \right] \\ &= \frac{\mathbf{p}^2}{2}, \end{aligned} \quad (\text{A19})$$

Hence the kinetic Weyl symbol equals $\mathbf{k}^2/2$ exactly. Combining the two pieces,

$$H_W(\boldsymbol{\theta}, \mathbf{p}) = \frac{\mathbf{p}^2}{2} + V(\boldsymbol{\theta}), \quad (\text{A20})$$

which is precisely the classical Hamiltonian of geometrical optics on $(\boldsymbol{\theta}, \mathbf{p})$. Because H_W is quadratic in \mathbf{p} and local in $\boldsymbol{\theta}$, the Moyal and Poisson brackets coincide exactly; thus the phase-space flow is a linear symplectic (metaplectic) map with no higher-order corrections.

Appendix B: Wigner function for polarised/coloured images

We extend the formalism for the Wigner function of a galaxy image so that it can analyse an image with polarisations/colours. Let us treat the image as a Jones field $\psi(\boldsymbol{\theta}) \in \mathbb{C}^2$ and define a 2×2 matrix-valued cross-Wigner

$$[W_{ab}^{\text{pol}}(z)]_{ij} = \frac{1}{(2\pi\lambda)^2} \int d^2\boldsymbol{\xi} \psi_{a,i}(\boldsymbol{\theta} + \boldsymbol{\xi}/2) \psi_{b,j}^*(\boldsymbol{\theta} - \boldsymbol{\xi}/2) e^{-\frac{i\mathbf{p}\cdot\boldsymbol{\xi}}{\lambda}}. \quad (\text{B1})$$

For a polarization basis change $U \in \text{U}(2)$ acting on components, one has

$$W_{Ua, Ub}^{\text{pol}}(z) = U W_{ab}^{\text{pol}}(z) U^\dagger, \quad (\text{B2})$$

so the total-intensity (scalar) cross-Wigner $\text{tr } W_{ab}^{\text{pol}}$ is basis-invariant. Thus polarization changes are genuinely unitary in this framework (rotations, phase retarders, Faraday rotation in a lossless model, etc.).

Two images of the same galaxy at different wavelengths need not be related by any unitary U on a common Hilbert space: the sky emission, PSF, and transfer function are chromatic and typically include non-unitary effects (convolution, absorption/emission). A useful exception is a pure first-order, lossless, paraxial change that is equivalent to a symplectic squeeze. Writing the symplectic squeeze $S_s = \text{diag}(sI_2, s^{-1}I_2)$ with metaplectic lift $\mu(S_s)$, one has

$$W_{\mu(S_s)a, \mu(S_s)b}(z) = W_{ab}(S_s^{-1}z). \quad (\text{B3})$$

In diffraction-limited optics, the core scale changes $\propto \lambda$; after non-dimensionalizing z so that λ is fixed, choosing $s \approx \sqrt{\lambda_2/\lambda_1}$ models the achromatic scaling between bands. Beyond this ideal case (e.g. band-dependent PSF, dust, stellar-population changes), no unitary map exists, and the cross-Wigner should be used as a comparative statistic rather than expected to obey simple covariance.

Appendix C: Derivation of the PSF phase-space kernel by direct variable changes

We derive the phase-space representation of PSF blurring directly from the configuration-space action by changing integration variables. Let $h(\boldsymbol{\theta})$ be the amplitude spread function, and let the morphology kernel be $\rho_I(\boldsymbol{\theta}_1, \boldsymbol{\theta}_2)$. The PSF acts bilinearly as

$$\rho_O(\boldsymbol{\theta}_1, \boldsymbol{\theta}_2) = \int d^2\boldsymbol{\theta}'_1 d^2\boldsymbol{\theta}'_2 h(\boldsymbol{\theta}_1 - \boldsymbol{\theta}'_1) h^*(\boldsymbol{\theta}_2 - \boldsymbol{\theta}'_2) \rho_I(\boldsymbol{\theta}'_1, \boldsymbol{\theta}'_2). \quad (\text{C1})$$

Inserting ρ_O into the Wigner transform Eq. (2), we obtain

$$\begin{aligned} W_O(\boldsymbol{\theta}, \mathbf{p}) &= \int d^2\boldsymbol{\xi} e^{-i\mathbf{p}\cdot\boldsymbol{\xi}/\lambda} \rho_O\left(\boldsymbol{\theta} + \frac{\boldsymbol{\xi}}{2}, \boldsymbol{\theta} - \frac{\boldsymbol{\xi}}{2}\right) \\ &= \int d^2\boldsymbol{\theta}_1 d^2\boldsymbol{\theta}_2 d^2\boldsymbol{\xi} e^{-i\mathbf{p}\cdot\boldsymbol{\xi}/\lambda} \\ &\quad \times h\left(\boldsymbol{\theta} + \frac{\boldsymbol{\xi}}{2} - \boldsymbol{\theta}_1\right) h^*\left(\boldsymbol{\theta} - \frac{\boldsymbol{\xi}}{2} - \boldsymbol{\theta}_2\right) \rho_I(\boldsymbol{\theta}_1, \boldsymbol{\theta}_2). \end{aligned} \quad (\text{C2})$$

Then, we change the variables in the integral with

$$\boldsymbol{\theta}' \equiv \frac{\boldsymbol{\theta}_1 + \boldsymbol{\theta}_2}{2}, \quad \boldsymbol{\eta} \equiv \boldsymbol{\theta}_1 - \boldsymbol{\theta}_2, \quad \mathbf{s} \equiv \boldsymbol{\xi} - \boldsymbol{\eta}. \quad (\text{C3})$$

One can confirm that the Jacobian stays unity. As the PSF factors depend only on $(\boldsymbol{\theta} - \boldsymbol{\theta}', \mathbf{s})$ and the phase splits as $e^{-i\mathbf{p}\cdot\boldsymbol{\xi}/\lambda} = e^{-i\mathbf{p}\cdot\mathbf{s}/\lambda} e^{-i\mathbf{p}\cdot\boldsymbol{\eta}/\lambda}$. Thus, W_O is rewritten as

$$\begin{aligned} W_O(\boldsymbol{\theta}, \mathbf{p}) &= \int d^2\boldsymbol{\theta}' d^2\boldsymbol{\eta} d^2\mathbf{s} \\ &\quad \times h\left(\boldsymbol{\theta} - \boldsymbol{\theta}' + \frac{\mathbf{s}}{2}\right) h^*\left(\boldsymbol{\theta} - \boldsymbol{\theta}' - \frac{\mathbf{s}}{2}\right) e^{-\frac{i\mathbf{p}\cdot\boldsymbol{\xi}}{\lambda}} \\ &\quad \times \rho_I\left(\boldsymbol{\theta}' + \frac{\boldsymbol{\eta}}{2}, \boldsymbol{\theta}' - \frac{\boldsymbol{\eta}}{2}\right) e^{-\frac{i\mathbf{p}\cdot\boldsymbol{\xi}}{\lambda}}. \end{aligned} \quad (\text{C4})$$

At this stage, it is more explicit that the integrals over \mathbf{s} and $\boldsymbol{\eta}$ respectively create the Wigner functions for each kernels $h(\boldsymbol{\theta} - \boldsymbol{\theta}') h^*(\boldsymbol{\theta} - \boldsymbol{\theta}')$ and $\rho_I(\boldsymbol{\theta}')$. Hence, the final expression becomes by representing $\boldsymbol{\theta} = \boldsymbol{\theta}^I$ as

$$W_O(\boldsymbol{\theta}, \mathbf{p}) = \int d\mu^I \Pi_{\text{PSF}}(\boldsymbol{\theta} - \boldsymbol{\theta}^I, \mathbf{p} - \mathbf{p}^I) W_I(\boldsymbol{\theta}^I, \mathbf{p}^I), \quad (\text{C5})$$

which is the desired form.

Appendix D: Determination of the normalisation of WFS

We determine the normalisation of the Wigner–function shapelet (WFS) basis so that the phase–space representation is consistent with the Hilbert–Schmidt (HS) inner product of operators.

We begin with the configuration-space inner product in Eq. (20) and the definition of the cross–Wigner function in Eq. (16). We consider the phase–space overlap

$$\mathcal{I} \equiv \int d^2\boldsymbol{\theta} d^2\mathbf{p} W_{ab}(\boldsymbol{\theta}, \mathbf{p}) W_{cd}^*(\boldsymbol{\theta}, \mathbf{p}). \quad (\text{D1})$$

Using $W_{cd}^* = W_{dc}$ and substituting the definition for both factors yields

$$\begin{aligned} \mathcal{I} &= \int d^2\boldsymbol{\theta} d^2\mathbf{p} \frac{1}{(2\pi\lambda)^4} \\ &\quad \times \int d^2\boldsymbol{\xi}_1 \int d^2\boldsymbol{\xi}_2 \psi_a\left(\boldsymbol{\theta} + \frac{\boldsymbol{\xi}_1}{2}\right) \psi_b^*\left(\boldsymbol{\theta} - \frac{\boldsymbol{\xi}_1}{2}\right) \\ &\quad \times \psi_c^*\left(\boldsymbol{\theta} + \frac{\boldsymbol{\xi}_2}{2}\right) \psi_d\left(\boldsymbol{\theta} - \frac{\boldsymbol{\xi}_2}{2}\right) e^{-\frac{i\mathbf{p}\cdot(\boldsymbol{\xi}_1-\boldsymbol{\xi}_2)}{\lambda}}. \end{aligned} \quad (\text{D2})$$

We now perform the \mathbf{p} integral first. The Fourier identity in two dimensions gives

$$\int d^2\mathbf{p} e^{-\frac{i\mathbf{p}\cdot(\boldsymbol{\xi}_1-\boldsymbol{\xi}_2)}{\lambda}} = (2\pi\lambda)^2 \delta^{(2)}(\boldsymbol{\xi}_1 - \boldsymbol{\xi}_2). \quad (\text{D3})$$

Inserting (D3) into (D2) collapses the $\boldsymbol{\xi}_2$ integral:

$$\begin{aligned} \mathcal{I} &= \frac{1}{(2\pi\lambda)^2} \int d^2\boldsymbol{\theta} \int d^2\boldsymbol{\xi} \psi_a\left(\boldsymbol{\theta} + \frac{\boldsymbol{\xi}}{2}\right) \psi_b^*\left(\boldsymbol{\theta} - \frac{\boldsymbol{\xi}}{2}\right) \\ &\quad \times \psi_c^*\left(\boldsymbol{\theta} + \frac{\boldsymbol{\xi}}{2}\right) \psi_d\left(\boldsymbol{\theta} - \frac{\boldsymbol{\xi}}{2}\right). \end{aligned} \quad (\text{D4})$$

At this stage it is convenient to change variables to the “endpoint” coordinates

$$\boldsymbol{x} \equiv \boldsymbol{\theta} + \frac{\boldsymbol{\xi}}{2}, \quad \boldsymbol{y} \equiv \boldsymbol{\theta} - \frac{\boldsymbol{\xi}}{2}. \quad (\text{D5})$$

This linear transformation is invertible with inverse dimensions, hence

$$d^2\boldsymbol{\theta} d^2\boldsymbol{\xi} = d^2\boldsymbol{x} d^2\boldsymbol{y}. \quad (\text{D6})$$

Therefore (D4) becomes

$$\begin{aligned} \mathcal{I} &= \frac{1}{(2\pi\lambda)^2} \int d^2\boldsymbol{x} \int d^2\boldsymbol{y} \psi_a(\boldsymbol{x}) \psi_c^*(\boldsymbol{x}) \psi_b^*(\boldsymbol{y}) \psi_d(\boldsymbol{y}) \\ &= \frac{1}{(2\pi\lambda)^2} \left[\int d^2\boldsymbol{x} \psi_a(\boldsymbol{x}) \psi_c^*(\boldsymbol{x}) \right] \left[\int d^2\boldsymbol{y} \psi_b^*(\boldsymbol{y}) \psi_d(\boldsymbol{y}) \right] \\ &= \frac{1}{(2\pi\lambda)^2} \langle \psi_a | \psi_c \rangle \langle \psi_b | \psi_d \rangle, \end{aligned} \quad (\text{D7})$$

which is precisely Eq. (21).

Appendix E: Analytic relation between LG modes and spherical harmonics at small-angle limit

We expand the derivation of how the LG mode $\Psi_{j,s}^{\text{LG}}$ analytically corresponds to the spherical harmonics $Y_{\ell m}$ at the small-angle limit, deriving the coefficient $\psi_{\ell}^{(j,s)}$ that is defined in Eq. (118). Let us recall that the spherical harmonics are approximated as Eq. (117). It is trivial that the angular mode is strictly based on the constraint $m = 2s$. For the radial mode, we employ the analytic integral identity as follows. The radial part of the LG mode is written as

$$R_{\nu}^{|\mu|}(x) \equiv \left(\sqrt{2}x\right)^{|\mu|} L_{\nu}^{|\mu|}(2x^2) e^{-x^2}, \quad (\text{E1})$$

where $L_{\nu}^{|\mu|}(x)$ denotes the associated Laguerre polynomial, $\nu \in \mathbb{N}_0$ is the radial index, $\mu \in \mathbb{Z}$ is the azimuthal index.

Let us introduce the Hankel transform of the radial LG mode admits the closed analytic form

$$\begin{aligned} \int_0^{\infty} dx x R_{\nu}^{|\mu|}(x) J_{|\mu|}(xy) &= \frac{(-1)^{\nu}}{2} \left(\frac{y}{\sqrt{2}}\right)^{|\mu|} L_{\nu}^{|\mu|}\left(\frac{y^2}{2}\right) e^{-\frac{y^2}{4}} \\ &= \frac{(-1)^{\nu}}{2} R_{\nu}^{|\mu|}\left(\frac{y}{2}\right). \end{aligned} \quad (\text{E2})$$

Note that Eq. (E2) exhibits a self similarity of the Hankel transform of $R_\nu^{|\mu|}(x)$. In order to extract the coefficient in Eq. (118), we use the orthogonality of the Bessel function

$$\int_0^\infty dx x J_\nu(ax) J_\nu(bx) = \frac{1}{a} \delta^D(a-b), \quad a, b > 0. \quad (\text{E3})$$

Appendix F: Weak-lensing operators with Swinger two oscillators

We adopt the standard Hamiltonian–Heisenberg convention in which an infinitesimal canonical transformation is generated by

$$\delta \hat{A} = \frac{1}{i\lambda} [\hat{A}, \hat{G}], \quad (\text{F1})$$

so that the classical limit is obtained by replacing commutators with Poisson brackets, $\delta A = \{A, G\}$.

a. Shear generator

In the circular (Schwinger) basis (\hat{a}_u, \hat{a}_v) , the gravitational shear is generated by a quadratic operator,

$$\hat{G}_\gamma = -\frac{i}{2} \gamma (\hat{a}_u^2 - \hat{a}_v^2) + \frac{i}{2} \gamma^* (\hat{a}_u^{\dagger 2} - \hat{a}_v^{\dagger 2}). \quad (\text{F2})$$

This yields

$$\delta \hat{a}_u = \gamma^* \hat{a}_u^\dagger, \quad \delta \hat{a}_v = \gamma \hat{a}_v^\dagger, \quad (\text{F3})$$

which reproduces, at the phase-space level, $\delta u = \gamma^* u^*$ and $\delta v = \gamma v^*$. The induced action on the Wigner function is therefore a Lie transport along the corresponding phase-space vector field.

b. Flexion generator

Flexion corresponds to the quadratic term in the lens mapping and is implemented as a canonical transformation generated by a cubic operator. In Cartesian variables, the universal form of the generator is

$$\hat{G}_{\text{flex}} = \frac{1}{2} D_{ijk} \widehat{p_i \theta_j \theta_k}, \quad (\text{F4})$$

where D_{ijk} is symmetric in (j, k) and $\widehat{\cdot \cdot \cdot}$ denotes a Hermitian (e.g. Weyl) ordering. This guarantees

$$\delta \hat{\theta}_i = \frac{1}{i\lambda} [\hat{\theta}_i, \hat{G}_{\text{flex}}] = \frac{1}{2} D_{ijk} \hat{\theta}_j \hat{\theta}_k, \quad (\text{F5})$$

with the corresponding momentum variation fixed by canonicity.

Let us define the complex operators $\hat{\theta} = \hat{\theta}_x + i\hat{\theta}_y$ and $\hat{p} = \hat{p}_x + i\hat{p}_y$, so that $[\hat{\theta}, \hat{p}^\dagger] = 2i\lambda$ and $[\hat{\theta}^\dagger, \hat{p}] = 2i\lambda$. A real Cartesian dot product can be written as $p_x \delta \theta_x + p_y \delta \theta_y = \Re(p^\dagger \delta \theta) = \frac{1}{2}(p^\dagger \delta \theta + p \delta \theta^\dagger)$. Hence an equivalent universal form of the flexion generator is

$$\hat{G}_{\text{flex}} = \Re(\hat{p}^\dagger \widehat{\delta \theta}) = \frac{1}{2} \hat{p}^\dagger \widehat{\delta \theta} + \widehat{\hat{p} \delta \theta^\dagger}, \quad (\text{F6})$$

with $\widehat{\cdot \cdot \cdot}$ denoting a Hermitian (e.g. Weyl) ordering. We identify the following operator as

$$\delta \hat{\theta} = \frac{1}{4} (2\mathcal{F} \hat{\theta} \hat{\theta}^\dagger + \mathcal{F}^* \hat{\theta}^2 + \mathcal{G} \hat{\theta}^{\dagger 2}), \quad (\text{F7})$$

The associated momentum update (Weyl symbol / classical form) is

$$\delta p = -\frac{1}{2} (\mathcal{F}^* \theta + \mathcal{F} \theta^*) p - \frac{1}{2} (\mathcal{F} \theta + \mathcal{G} \theta^*) p^*, \quad (\text{F8})$$

with the operator expression obtained by the same Hermitian ordering.

The flexion moment as

$$\delta \theta = \frac{1}{4} (2\mathcal{F} |\theta|^2 + \mathcal{F}^* \theta^2 + \mathcal{G} \theta^{*2}). \quad (\text{F9})$$

We can derive the corresponding variation of the complex conjugate momentum as

$$\delta p = -\frac{\mathcal{F}}{2} (\theta p^* + \theta^* p) - \frac{\mathcal{F}^*}{2} \theta p - \frac{\mathcal{G}}{2} \theta^* p^*. \quad (\text{F10})$$

Here we denote $\mathcal{F} = [\Phi_{xxx} + \Phi_{xyy} + i(\Phi_{xxy} + \Phi_{yyx})]/2$ and $\mathcal{G} = [\Phi_{xxx} - 3\Phi_{xyy} + i(3\Phi_{xxy} - \Phi_{yyx})]/2$, where $\Phi_{xxy} = \Phi_{xyx} = \Phi_{yxx}$. For simplicity in this appendix, we employ the unit $\sigma = 1$, including the effect of the magnification. One can recover the scaling of σ , rescaling $\mathcal{F} \rightarrow \mathcal{F}\sigma^2$ and $\mathcal{G} \rightarrow \mathcal{G}\sigma^2$. The induced action on phase space again takes the form of a Lie derivative, providing a direct extension of the shear case. A Hermitian universal form of the flexion generator is $\hat{G}_{\text{flex}} = \Re(\hat{p}^\dagger \widehat{\delta \theta})$ with

$$\delta \hat{\theta} = \frac{1}{4} (2\mathcal{F} \hat{\theta} \hat{\theta}^\dagger + \mathcal{F}^* \hat{\theta}^2 + \mathcal{G} \hat{\theta}^{\dagger 2}), \quad (\text{F11})$$

where $\widehat{\cdot \cdot \cdot}$ denotes a Hermitian (e.g. Weyl) ordering. Substituting the above dictionary yields $\hat{G}_{\text{flex}} = \hat{G}_{\mathcal{F}} + \hat{G}_{\mathcal{G}}$ with

$$\begin{aligned}
\hat{G}_{\mathcal{G}} &= \frac{i\lambda}{8\sqrt{2}} \left[-\mathcal{G} \left(\hat{a}_u^3 + \hat{a}_u^2 \hat{a}_v^\dagger - \hat{a}_u \hat{a}_v^{\dagger 2} - \hat{a}_v^{\dagger 3} \right) + \mathcal{G}^* \left(\hat{a}_u^{\dagger 3} + \hat{a}_u^{\dagger 2} \hat{a}_v - \hat{a}_u^\dagger \hat{a}_v^2 - \hat{a}_v^3 \right) \right], \\
\hat{G}_{\mathcal{F}} &= \frac{i\lambda}{8\sqrt{2}} \left[-\mathcal{F} \left(\hat{a}_u^2 \hat{a}_u^\dagger + 3 \hat{a}_u^2 \hat{a}_v - 2 \hat{a}_u \hat{a}_u^\dagger \hat{a}_v^\dagger + 2 \hat{a}_u \hat{a}_v \hat{a}_v^\dagger - 3 \hat{a}_u^\dagger \hat{a}_v^{\dagger 2} - \hat{a}_v \hat{a}_v^{\dagger 2} \right) \right. \\
&\quad \left. + \mathcal{F}^* \left(\hat{a}_u \hat{a}_u^{\dagger 2} - 3 \hat{a}_u \hat{a}_v^2 - 2 \hat{a}_u \hat{a}_u^\dagger \hat{a}_v + 2 \hat{a}_u^\dagger \hat{a}_v \hat{a}_v^\dagger + 3 \hat{a}_u^{\dagger 2} \hat{a}_v^\dagger - \hat{a}_v^2 \hat{a}_v^\dagger \right) \right]. \tag{F12}
\end{aligned}$$

Then we derive

$$\begin{aligned}
\delta \hat{a}_u &= \frac{\mathcal{F}^*}{4\sqrt{2}} (\hat{a}_u \hat{a}_u^\dagger + 3 \hat{a}_u^\dagger \hat{a}_v^\dagger - \hat{a}_u \hat{a}_v + \hat{a}_v \hat{a}_v^\dagger) + \frac{\mathcal{F}}{8\sqrt{2}} (3 \hat{a}_v^{\dagger 2} + 2 \hat{a}_u \hat{a}_v^\dagger - \hat{a}_u^2) + \frac{\mathcal{G}^*}{8\sqrt{2}} (3 \hat{a}_u^{\dagger 2} + 2 \hat{a}_u^\dagger \hat{a}_v - \hat{a}_v^2), \\
\delta \hat{a}_v &= \frac{\mathcal{F}}{4\sqrt{2}} (\hat{a}_u \hat{a}_u^\dagger + 3 \hat{a}_u^\dagger \hat{a}_v^\dagger - \hat{a}_u \hat{a}_v + \hat{a}_v \hat{a}_v^\dagger) + \frac{\mathcal{F}^*}{8\sqrt{2}} (3 \hat{a}_u^{\dagger 2} + 2 \hat{a}_u^\dagger \hat{a}_v - \hat{a}_v^2) + \frac{\mathcal{G}}{8\sqrt{2}} (3 \hat{a}_v^{\dagger 2} + 2 \hat{a}_u \hat{a}_v^\dagger - \hat{a}_u^2), \tag{F13}
\end{aligned}$$

and equivalently

$$\begin{aligned}
\frac{\delta u}{u} &= \frac{\mathcal{F}^*}{4\sqrt{2}|u|} ((|u|^2 + |v|^2) \chi_{-1,0} + 3|u||v| \chi_{-2,-1} - |u||v| \chi_{0,1}) \\
&\quad + \frac{\mathcal{F}}{8\sqrt{2}|u|} (3|v|^2 \chi_{-1,-2} + 2|u||v| \chi_{0,-1} - |u|^2 \chi_{1,0}) + \frac{\mathcal{G}^*}{8\sqrt{2}|u|} (3|u|^2 \chi_{-3,0} + 2|u||v| \chi_{-2,1} - |v|^2 \chi_{-1,2}), \\
\frac{\delta v}{v} &= \frac{\mathcal{F}}{4\sqrt{2}|v|} ((|u|^2 + |v|^2) \chi_{0,-1} + 3|u||v| \chi_{-1,-2} - |u||v| \chi_{1,0}) \\
&\quad + \frac{\mathcal{F}^*}{8\sqrt{2}|v|} (3|u|^2 \chi_{-2,-1} + 2|u||v| \chi_{-1,0} - |v|^2 \chi_{0,1}) + \frac{\mathcal{G}}{8\sqrt{2}|v|} (3|v|^2 \chi_{0,-3} + 2|u||v| \chi_{1,-2} - |u|^2 \chi_{2,-1}), \tag{F14}
\end{aligned}$$

After carefully treating the phase integration, we obtain the flexion response function as

$$\begin{aligned}
\mathcal{W}_{k\ell}^I(Q_0, Q_2) - \mathcal{W}_{k\ell}^S(Q_0, Q_2) &= A_{k\ell}^{\mathcal{F}} \mathcal{F} + A_{k\ell}^{\mathcal{F}^*} \mathcal{F}^* + A_{k\ell}^{\mathcal{G}} \mathcal{G} + A_{k\ell}^{\mathcal{G}^*} \mathcal{G}^* , \\
A_{k\ell}^{\mathcal{F}} &= \frac{1}{8\sqrt{2}|u|} \left[-(|u|^2 + |v|^2)(|u|\partial_{|u|} - (k-1))\mathcal{W}_{k-1,\ell}^S - 3|u||v|(|u|\partial_{|u|} - (k-2))\mathcal{W}_{k-2,\ell-1}^S + |u||v|(|u|\partial_{|u|} - k)\mathcal{W}_{k,\ell+1}^S \right] \\
&\quad + \frac{1}{16\sqrt{2}|u|} \left[|u|^2(|u|\partial_{|u|} + (k-1))\mathcal{W}_{k-1,\ell}^S - |u||v|(|u|\partial_{|u|} + k)\mathcal{W}_{k,\ell+1}^S - |v|^2(|u|\partial_{|u|} + (k+1))\mathcal{W}_{k+1,\ell+2}^S \right] \\
&\quad + \frac{1}{16\sqrt{2}|v|} \left[-3|u|^2(|v|\partial_{|v|} - (\ell-1))\mathcal{W}_{k-2,\ell-1}^S - |u||v|(|v|\partial_{|v|} - \ell)\mathcal{W}_{k-1,\ell}^S + |v|^2(|v|\partial_{|v|} - (\ell+1))\mathcal{W}_{k,\ell+1}^S \right] \\
&\quad + \frac{1}{8\sqrt{2}|v|} \left[-(|u|^2 + |v|^2)(|v|\partial_{|v|} + (\ell+1))\mathcal{W}_{k,\ell+1}^S - 3|u||v|(|v|\partial_{|v|} + (\ell+2))\mathcal{W}_{k+1,\ell+2}^S + |u||v|(|v|\partial_{|v|} + \ell)\mathcal{W}_{k-1,\ell}^S \right] \\
A_{k\ell}^{\mathcal{F}^*} &= \frac{1}{8\sqrt{2}|u|} \left[-(|u|^2 + |v|^2)(|u|\partial_{|u|} + (k+1))\mathcal{W}_{k+1,\ell}^S - 3|u||v|(|u|\partial_{|u|} + (k+2))\mathcal{W}_{k+2,\ell+1}^S + |u||v|(\partial_{|u|} + k)\mathcal{W}_{k,\ell-1}^S \right] \\
&\quad + \frac{1}{16\sqrt{2}|u|} \left[|u|^2(|u|\partial_{|u|} - (k+1))\mathcal{W}_{k+1,\ell}^S - |u||v|(|u|\partial_{|u|} - k)\mathcal{W}_{k,\ell-1}^S - |v|^2(|u|\partial_{|u|} - (k-1))\mathcal{W}_{k-1,\ell-2}^S \right] , \\
&\quad + \frac{1}{16\sqrt{2}|v|} \left[-3|u|^2(|v|\partial_{|v|} + (\ell+1))\mathcal{W}_{k+2,\ell+1}^S - |u||v|(|v|\partial_{|v|} + \ell)\mathcal{W}_{k+1,\ell}^S + |v|^2(|v|\partial_{|v|} + (\ell-1))\mathcal{W}_{k,\ell-1}^S \right] , \\
&\quad - \frac{1}{8\sqrt{2}|v|} \left[-(|u|^2 + |v|^2)(|v|\partial_{|v|} - (\ell-1))\mathcal{W}_{k,\ell-1}^S - 3|u||v|(|v|\partial_{|v|} - (\ell-2))\mathcal{W}_{k-1,\ell-2}^S + |u||v|(|v|\partial_{|v|} - \ell)\mathcal{W}_{k+1,\ell}^S \right] \\
A_{k\ell}^{\mathcal{G}} &= \frac{1}{16\sqrt{2}|u|} \left[-3|u|^2(|u|\partial_{|u|} - (k-3))\mathcal{W}_{k-3,\ell}^S - 2|u||v|(|u|\partial_{|u|} - (k-2))\mathcal{W}_{k-2,\ell+1}^S + |v|^2(|u|\partial_{|u|} - (k-1))\mathcal{W}_{k-1,\ell+2}^S \right] \\
&\quad + \frac{1}{16\sqrt{2}|v|} \left[-3|u|^2(|v|\partial_{|v|} + (\ell+3))\mathcal{W}_{k,\ell+3}^S - 2|u||v|(|v|\partial_{|v|} + (\ell+1))\mathcal{W}_{k-1,\ell+2}^S + |v|^2(|v|\partial_{|v|} + (\ell+1))\mathcal{W}_{k-2,\ell+1}^S \right] , \\
A_{k\ell}^{\mathcal{G}^*} &= \frac{1}{16\sqrt{2}|u|} \left[-3|u|^2(|u|\partial_{|u|} + (k+3))\mathcal{W}_{k+3,\ell}^S - 2|u||v|(|u|\partial_{|u|} + (k+2))\mathcal{W}_{k+2,\ell-1}^S + |v|^2(|u|\partial_{|u|} + (k+1))\mathcal{W}_{k+1,\ell-2}^S \right] \\
&\quad + \frac{1}{16\sqrt{2}|v|} \left[-3|u|^2(|u|\partial_{|v|} - (\ell-3))\mathcal{W}_{k,\ell-3}^S - 2|u||v|(|v|\partial_{|v|} - (\ell-1))\mathcal{W}_{k+1,\ell-2}^S + |v|^2(|v|\partial_{|v|} - (\ell-1))\mathcal{W}_{k+2,\ell-1}^S \right] ,
\end{aligned}
\tag{F15}$$

- [1] A. Refregier, *Mon. Not. R. Astron. Soc.* **338**, 35 (2003).
- [2] A. Refregier and D. Bacon, *Mon. Not. R. Astron. Soc.* **338**, 48 (2003).
- [3] R. Massey and A. Refregier, *Mon. Not. R. Astron. Soc.* **363**, 197 (2005).
- [4] R. Massey, B. Rowe, A. Refregier, D. J. Bacon, and J. Bergé, *Mon. Not. R. Astron. Soc.* **380**, 229 (2007), arXiv:astro-ph/0609795 [astro-ph].
- [5] R. Mandelbaum, *Ann. Rev. Astron. Astrophys.* **56**, 393 (2018), arXiv:1710.03235 [astro-ph.CO].
- [6] D. J. Bacon, D. M. Goldberg, B. T. P. Rowe, and A. N. Taylor, *Mon. Not. Roy. Astron. Soc.* **365**, 414 (2006), arXiv:astro-ph/0504478.
- [7] X. Li, N. Katayama, M. Oguri, and S. More, *Mon. Not. R. Astron. Soc.* **481**, 4445 (2018), arXiv:1805.08514 [astro-ph.CO].
- [8] X. Li, Y. Li, and R. Massey, *Mon. Not. R. Astron. Soc.* **511**, 4850 (2022), arXiv:2110.01214 [astro-ph.CO].
- [9] J. P. Gardner, J. C. Mather, M. Clampin, R. Doyon, M. A. Greenhouse, H. B. Hammel, J. B. Hutchings, P. Jakobsen, S. J. Lilly, K. S. Long, J. I. Lunine, M. J. McCaughrean, M. Mountain, J. Nella, G. H. Rieke, M. J. Rieke, H.-W. Rix, E. P. Smith, G. Sonneborn, M. Stiavelli, H. S. Stockman, R. A. Windhorst, and G. S. Wright, *Space Sci. Rev.* **123**, 485 (2006).
- [10] R. Laureijs et al., *arXiv e-prints* (2011), arXiv:1110.3193 [astro-ph.CO].
- [11] LSST Science Collaboration, *LSST Science Book, Version 2.0* (arXiv e-prints, 2009) arXiv:0912.0201 [astro-ph.IM].
- [12] R. Braun et al., *arXiv e-prints* (2019), arXiv:1912.12699 [astro-ph.IM].
- [13] D. Spergel, N. Gehrels, C. Baltay, D. Bennett, J. Breckinridge, M. Donahue, A. Dressler, B. S. Gaudi, T. Greene, O. Guyon, C. Hirata, J. Kalirai, N. J. Kasdin, W. Moos, S. Perlmutter, M. Postman, B. Rauscher, J. Rhodes, Y. Wang, D. Weinberg, D. Benford, M. Hudson, W. Jeong, Y. Mellier, W. Traub, T. Yamada, S. Capak, J. Colbert, D. Masters, M. Penny, D. Savransky, D. Stern, N. Zimmerman, R. Barry, L. Bartusek, K. Carpenter, E. Cheng, D. Content, F. Dekens, R. Demers,

K. Grady, C. Jackson, G. Kuan, M. Kuyat, J. Lamborn, M. Nemati, B. Parvin, I. Poberezhskiy, B. Peddie, S. Ruffa, J. Wallace, A. Whipple, E. Wollack, and F. Zhao, arXiv e-prints (2015), arXiv:1503.03757 [astro-ph.IM].

[14] A. Tagore and C. Keeton, *Mon. Not. Roy. Astron. Soc.* **445**, 694 (2014), arXiv:1408.6297 [astro-ph.CO].

[15] N. Ephremidze, C. Chandrashekhar, A. Çağan Şengül, and C. Dvorkin, arXiv e-prints, arXiv:2502.18571 (2025), arXiv:2502.18571 [astro-ph.CO].

[16] S. Yatawatta, *Astron. Astrophys.* (2024), open access.

[17] G. Nienhuis, *Phys. Rev. A* **48**, 656 (1993).

[18] A. R. Edmonds, *Angular Momentum in Quantum Mechanics* (Princeton University Press, 1957) foundational text on angular momentum theory; see also review by H. C. Bolton (1959).

[19] D. A. Varshalovich, A. N. Moskalev, and V. K. Khersonskii, *Quantum Theory of Angular Momentum* (World Scientific, 1988).

[20] E. P. Wigner, *Group Theory and its Application to the Quantum Mechanics of Atomic Spectra*, Pure and Applied Physics, Vol. 5 (Academic Press, New York, 1959) expanded and improved edition; translated by J. J. Griffin.

[21] L. Allen, M. W. Beijersbergen, R. J. C. Spreeuw, and J. P. Woerdman, *Phys. Rev. A* **45**, 8185 (1992).

[22] P. A. M. Dirac, *The Principles of Quantum Mechanics*, 1st ed. (Oxford University Press, Oxford, 1930) landmark text in quantum mechanics; reviewed in Lennard-Jones (1931) *Mathematical Gazette*.

[23] C. Cohen-Tannoudji, B. Diu, and F. Laloë, *Quantum Mechanics* (Wiley, New York, 1997) standard graduate-level textbook; listed as core text in MIT OCW quantum mechanics syllabus (Fall 2018).

[24] E. P. Wigner, *Phys. Rev.* **40**, 749 (1932).

[25] J. Ville, *Câbles et Transmissions* **2**, 61 (1948), in French; introduces the analytic signal formalism.

[26] W. P. Schleich, *Quantum Optics in Phase Space* (Wiley-VCH, 2001).

[27] U. Leonhardt, *Measuring the Quantum State of Light* (Cambridge University Press, 1997).

[28] A. I. Lvovsky and M. G. Raymer, *Rev. Mod. Phys.* **81**, 299 (2009).

[29] C. Weedbrook, S. Pirandola, R. García-Patrón, N. J. Cerf, T. C. Ralph, J. H. Shapiro, and S. Lloyd, *Rev. Mod. Phys.* **84**, 621 (2012).

[30] H. J. Groenewold, *Physica* **12**, 405 (1946).

[31] J. E. Moyal, *Proc. Cambridge Philos. Soc.* **45**, 99 (1949).

[32] R. Simon and G. S. Agarwal, *Optics Letters* **25**, 1313 (2000).

[33] H. Weyl, *The Theory of Groups and Quantum Mechanics* (Dover, New York, 1950) english translation by H. P. Robertson of the German original: H. Weyl, “Quantenmechanik und Gruppentheorie,” *Z. Phys.* 46, 1 (1927).

[34] R. L. Stratton, Sov. Phys. JETP **31**, 1012 (1956).

[35] J. C. Várilly and J. M. Gracia-Bondía, *Ann. Phys.* **190**, 107 (1989).

[36] C. Brif and A. Mann, *Phys. Rev. A* **59**, 971 (1999).

[37] M. Hillery, R. F. O’Connell, M. O. Scully, and E. P. Wigner, *Phys. Rep.* **106**, 121 (1984).

[38] G. B. Folland, *Harmonic Analysis in Phase Space*, Annals of Mathematics Studies, Vol. 122 (Princeton University Press, Princeton, NJ, 1989) p. 288, published Mar 21, 1989.

[39] H. Hopf, *Math. Ann.* **104**, 637 (1931).

[40] H. Kogelnik and T. Li, *Appl. Opt.* **5**, 1550 (1966).

[41] A. E. Siegman, *Lasers* (University Science Books, 1986).

[42] M. Born and E. Wolf, *Principles of Optics*, 7th ed. (Cambridge University Press, Cambridge, 1999).

[43] D. J. Schroeder, *Astronomical Optics*, 2nd ed. (Academic Press, San Diego, 2000).

[44] E. Hecht, *Optics*, 4th ed. (Addison Wesley, San Francisco, 2002).

[45] D. Manzano, *AIP Advances* **10**, 025106 (2020), arXiv:1906.04478 [quant-ph].

[46] P. H. van Cittert, *Physica* **1**, 201 (1934).

[47] F. Zernike, *Physica* **5**, 785 (1938).

[48] J. W. Goodman, *Statistical Optics* (Wiley, New York, 1985).

[49] J. W. Goodman, *Journal of the Optical Society of America* **66**, 1145 (1976).

[50] J. W. Goodman, *Introduction to Fourier Optics*, 3rd ed. (Roberts and Company, Greenwood Village, CO, 2005).

[51] R. Cerbino, *Physical Review A* **75**, 053815 (2007).

[52] A. J. F. Siegert, *On the Fluctuations in Signals Returned by Many Independently Moving Scatterers*, Tech. Rep. 465 (MIT Radiation Laboratory, 1943).

[53] M. Lax, *Reviews of Modern Physics* **32**, 25 (1960).

[54] R. Hanbury Brown and R. Q. Twiss, *Nature* **177**, 27 (1956).

[55] R. Hanbury Brown and R. Q. Twiss, *Proceedings of the Royal Society of London Series A* **242**, 300 (1957).

[56] D. A. Varshalovich, A. N. Moskalev, and V. K. Khersonskii, *Quantum Theory of Angular Momentum* (1988).

[57] N. Joshi, S. Jhingan, T. Souradeep, and A. Hajian, *Phys. Rev. D* **81**, 083012 (2010), arXiv:0912.3217 [astro-ph.CO].

[58] L. G. Book, M. Kamionkowski, and T. Souradeep, *Phys. Rev. D* **85**, 023010 (2012), arXiv:1109.2910 [astro-ph.CO].

[59] T. Kurita, D. Jamieson, E. Komatsu, and F. Schmidt, arXiv e-prints, arXiv:2509.08787 (2025), arXiv:2509.08787 [astro-ph.CO].

[60] W. Heisenberg, *Zeitschrift für Physik* **43**, 172 (1927).

[61] E. H. Kennard, *Zeitschrift für Physik* **44**, 326 (1927).

[62] H. P. Robertson, *Physical Review* **34**, 163 (1929).

[63] P. Jordan, *Zeitschrift für Physik* **94**, 531 (1935).

[64] J. S. Schwinger, *On Angular Momentum*, Tech. Rep. NYO-3071 (U.S. Atomic Energy Commission, 1952) technical Report;

reprinted in L.C.Biedenharn and H.Van Dam (eds.), **Quantum Theory of Angular Momentum** (Academic Press, 1965) and in K.A.Milton (ed.), **A Quantum Legacy** (World Scientific, 2000).

[65] L. Poh-aun, S.-H. Ong, and H. Srivastava, *International Journal of Computer Mathematics* **78**, 303 (2001).

[66] E. Komatsu, *Nature Reviews Physics* **4**, 452 (2022), arXiv:2202.13919 [astro-ph.CO].

[67] O. H. E. Philcox, M. J. König, S. Alexander, and D. N. Spergel, *Phys. Rev. D* **109**, 063541 (2024), arXiv:2309.08653 [astro-ph.CO].

[68] J. Zhang, *Mon. Not. R. Astron. Soc.* **383**, 113 (2008), arXiv:astro-ph/0612146 [astro-ph].

[69] D. J. Bacon, D. M. Goldberg, B. T. P. Rowe, and A. N. Taylor, *Mon. Not. R. Astron. Soc.* **365**, 414 (2006), arXiv:astro-ph/0504478 [astro-ph].

[70] Y. Okura and T. Futamase, *Mon. Not. R. Astron. Soc.* **516**, 668 (2022), arXiv:2109.00155 [astro-ph.CO].

[71] Y. Minami and E. Komatsu, *Astrophys. J. Lett.* **902**, L22 (2020), apJ Lett. 902, L22 (2020).

[72] F. Naokawa, *arXiv e-prints*, arXiv:2504.06709 (2025), arXiv:2504.06709 [astro-ph.CO].

[73] Y. Minami and E. Komatsu, *Phys. Rev. Lett.* **125**, 221301 (2020), arXiv:2011.11254 [astro-ph.CO].

[74] C. Hirata and U. Seljak, *Mon. Not. R. Astron. Soc.* **343**, 459 (2003), arXiv:astro-ph/0301054 [astro-ph].

[75] A. R. Thompson, J. M. Moran, and G. W. Swenson, *Interferometry and Synthesis in Radio Astronomy* (Springer, 2017).

[76] J. W. Goodman, *Introduction to Fourier Optics* (Roberts & Company, 2005).

[77] J. E. Krist, R. N. Hook, and F. Stoehr, *PASP* **117**, 594 (2005).

[78] J. W. Hardy, *Adaptive Optics for Astronomical Telescopes* (Oxford University Press, 1998).

[79] J. R. Janesick, *Scientific Charge-Coupled Devices* (SPIE Press, 2001).

[80] D. Petz, *Communications in Mathematical Physics* **105**, 123 (1986).

[81] A. Mokeev, B. Saif, M. D. Lukin, and J. Borregaard, *arXiv e-prints*, arXiv:2509.09465 (2025), arXiv:2509.09465 [quant-ph].

[82] M. Kalash and M. V. Chekhova, *Optica* **10**, 1142 (2023), arXiv:2207.10030 [quant-ph].

[83] N. K. Fontaine, R. Ryf, H. Chen, D. T. Neilson, K. Kim, and J. Carpenter, *Nature Communications* **10**, 1865 (2019), arXiv:1803.04126 [physics.optics].

[84] G. Galilei, *Sidereus Nuncius, or The Sidereal Messenger* (University of Chicago Press, Chicago, 1989) translated by Albert Van Helden.

[85] C. Huygens, *Systema Saturnium* (Adrian Vlacq, The Hague, 1659) first detailed description of Saturn's system; includes Mars sketches.

[86] G. D. Cassini, *Découverte de la division de l'anneau de Saturne* (Académie des Sciences, Paris, 1675) memoir reporting discovery of the Cassini Division.

[87] W. Herschel, *Scientific Papers of Sir William Herschel*, Vol. 1 (Royal Society and Royal Astronomical Society, London, 1912) collected works, including nebula and cluster morphology.

[88] E. P. Hubble, *Astrophys. J.* **64**, 321 (1926).

[89] E. P. Hubble, *The Realm of the Nebulae* (Yale University Press, New Haven, 1936).

[90] F. Zwicky, *Morphological Astronomy* (Springer, Berlin, 1957).

[91] G. de Vaucouleurs, *Handbuch der Physik* **53**, 275 (1959).

[92] M. Steinmetz and J. F. Navarro, *New Astron. Rev.* **46**, 699 (2002).

[93] C. J. Conselice, *Ann. Rev. Astron. Astrophys.* **52**, 291 (2014).

[94] R. J. Buta, *Proc. Int. Astron. Union* **6**, 171 (2010).

[95] C. J. Lintott, K. Schawinski, A. Slosar, K. Land, S. Bamford, D. Thomas, M. J. Raddick, R. C. Nichol, A. Szalay, D. Andreescu, P. Murray, and J. Vandenberg, *Mon. Not. R. Astron. Soc.* **389**, 1179 (2008).

[96] K. G. Iyer, P. Behroozi, J. R. Primack, D. J. Wilkins, A. Dekel, and D. Ceverino, *Astron. Astrophys.* **684**, A33 (2024).

[97] S. Bag, S. Bharadwaj, S. Sarkar, and S. K. Pandey, *Mon. Not. R. Astron. Soc.* **508**, 2765 (2021).

[98] Event Horizon Telescope Collaboration, *Astrophys. J. Lett.* **875**, L1 (2019).

[99] M. Bartelmann and P. Schneider, *Phys. Rep.* **340**, 291 (2001).

[100] M. Kilbinger, *Rep. Prog. Phys.* **78**, 086901 (2015).

[101] A. Lue, L. Wang, and M. Kamionkowski, *Phys. Rev. Lett.* **83**, 1506 (1999).